Morphology, Structure, and Magnetic Properties of Nanocrystalline Zinc Substituted Manganese Ferrites Synthesized by Coprecipitation

By

Pooja Srivastava

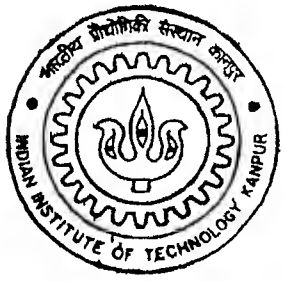

MATERIALS SCIENCE PROGRAMME

Indian Institute of Technology Kanpur

JULY 2002

Morphology, Structure, and Magnetic Properties of Nanocrystalline Zinc Substituted Manganese Ferrites Synthesized by Coprecipitation

A thesis submitted
in partial fulfillment of the requirement
for the degree of

Master of Technology

by

Pooja Srivastava

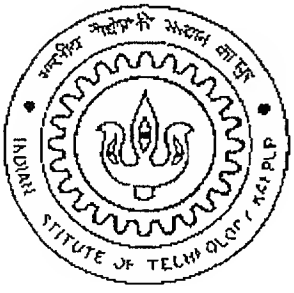

Materials Science Programme
Indian Institute of Technology, Kanpur
July, 2002

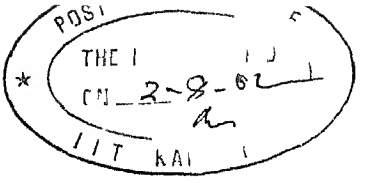

CERTIFICATE

It is certified that the work contained in this thesis entitled **"Morphology, Structure, and Magnetic Properties of Nanocrystalline Zinc Substituted Manganese Ferrites Synthesized by Coprecipitation"** by Pooja Srivastava has been carried out under my supervision and this work has not been submitted elsewhere for a degree

Jitendra Kumar

(Jitendra Kumar)

Professor

Materials Science Programme

Indian Institute of Technology

Kanpur 208016

July 2002

Acknowledgement

I am deeply indebted to my supervisor Prof Jitendra Kumar for his inspiring guidance during the course of thesis work He has constantly encouraged me and he has been very cooperative and understanding I feel fortunate that I have been under his tutelage

I pay my sincere gratitude to Prof K N Rai for his invaluable guidance and continuous encouragement

I am very grateful to Aditi, Pallavi Ruchi Pratibha Dhananjay, and Muthukumaran for their help and support towards the completion of this work

I would like to give thanks to my friends Aditi Datta Pallavi, Ruchi, Anurag Dulal Sanjay Tathagat Gopinath, Rahul and Praveendra for maintaining the cordial and friendly environment throughout the course period and there after

I would like to extend my sincere thanks to Aditi Agarwal Sweta Nidhi Medini and Pratibha for constant support encouragement and making my stay in hostel a very pleasant memory Thanks are due to all of my friends who gave a memorable and enjoyable company throughout my stay

I appreciate Thapaji for his timely help during my experimental work

I give special thanks to Uma Shankarji Sharmaji, Shiv Kumarji, Barthawalji and Paul for their constant help throughout the experiments

Finally I would like to give special thanks to my parents, sister and brother for their encouragement and moral support

Pooja Srivastava

Abstract

Zinc substituted manganese ferrites of composition $Mn_{1-x}Zn_x Fe_2O_4$ ($0 \leq x \leq 0.5$) have been investigated with regard to their phase(s) surface area and magnetic properties. It is shown that coprecipitation of metal salts taking sodium hydroxide as a reaction agent followed by digestion at 90^0C for 90 minutes and calcination at 200^0C for 2h yields successfully nanocrystalline particles of average diameter 6-10.2 nm. They contain a single phase having an f.c.c. structure with lattice parameter decreasing with increasing zinc content (the values being 8.503±0.001Å and 8.419±0.001Å for x = 0 and 0.5 respectively). Transmission electron microscopic observations have been extended to confirm the nano crystalline nature of the products. BET specific surface area is found to increase from 118.2 to 194.2 m^2/g for zinc content x = 0 to 0.4 indicating emergence of progressively smaller crystallites.

Pure $MnFe_2O_4$ particles exhibit low saturation magnetization M_s (~42.98 emu/g) and high Curie temperature T_C (378^0C) in comparison to bulk, the values of M_s and T_C being 80 emu/g and 300^0C respectively. Zinc substitution causes overall lowering of saturation magnetization, depicting a value of 22.15 emu/g only for x=0.2. With further increase in zinc content, M_s value increases to 28.8 emu/g and 35.16 emu/g for x=0.3 and 0.4 respectively but decreases sharply to 16.94 emu/g for x=0.5. The lowering of saturation magnetization and enhancement of Curie temperature are attributed to continuous decrease of particle size, cation redistribution and/or presence of a magnetic dead layer on the surface.

CONTENTS

List of Figures

List of Tables

Chapter 1
Introduction

Ultrafine magnetic particles have received attention and generated renewed interest in recent past because of their potential applications in nanostructured materials technology such as magnetic recording [1 2 3 4] earth s field mapping satellite [5] cryogenic technology [6] imaging technique [7] biology and medical diagnosis [8] high frequency devices [9] etc These particles exhibit properties which are sometimes found to be drastically different from those of corresponding bulk materials and arise mainly due to their reduced size (hence large surface area) pronounced surface effects and nature of magnetic interaction [10]

Magnetic materials are those materials that can be attracted or repelled by a magnet. The materials when placed in magnetic field cause change in flux or lines of forces (ϕ) and are accordingly classified as dia- para ferro anti-ferro and ferri magnetic (Table 1 1) When ϕ increase the material is considered to be magnetized On switching off the magnetic field material may or may not get demagnetized The parameter that characterized magnetic materials includes saturation magnetization (M_s) permeability (μ) transition temperature (Cur ie Neel) Coercive field (H_c) nature of hysteresis loop [11]

Table 1 1 Classification of magnetic materials [11]

S No	Type	Change in flux	Example(s)
1	Diamagnetic	Decreases	Cu, He
2	Paramagnetic	Increases marginally	Na Al
3	Ferromagnetic	Increases largely	Fe Co Ni
4	Antiferromagnetic	Increases reasonably	MnO FeO
5	ferrimagnetic	Increases largely	Fe_3O_4

The magnetic materials can be further divided into two main groups, soft and hard materials depending on their being magnetized and demagnetized easily and with difficulty, respectively The distinguishing characteristics of the soft material is their high permeability, narrow hysteresis loop (or low energy loss), low coercivity, low eddy current losses and high saturation induction/flux multiplying power A few examples are pure iron, low carbon steels, Fe-Ni alloys, spinel (ferrite such as Ni-Zn, Mn-Fe and Ni-Co ferrites) hexagonal ferrites synthetic garnets etc Some properties of soft magnetic materials are listed in the Table 1 2 In contrast hard materials show high coercivity wide hysteresis loop(high energy loss), resistance to demagnetizing action, etc These are essentially permanent magnet Some

examples include high carbon steel Fe Pt Pt Co hard ferrites rare earth containing alloys etc [12] The properties of selected hard magnetic materials are listed in Table 1 3

Among magnetic materials ferrites make a very important class and are basically double oxides of iron and another metal These are essentially ionic compounds and their characteristic properties arise due to magnetic ions present

Table1 2 Properties of soft magnetic materials [12]

Chemical formula/composition (wt%)	Curie temperature T_c (°C)	Maximum magnetic permeability μ_{max} (μ_o)	Remanence magnetic induction, B_R (Tesla)	Coercive magnetic field Hc ($A\ m^{-1}$)	Saturation magnetization Bs	Electrical resistivity ρ (μΩcm)
Fe	770	6000 8000	0 11-0 58	32 70	2 158	10
99Fe 1Si	740	7700	0 80 1 10	44	2 10	25
(Ni Zn)Fe_2O_4	–	–	0 11	14 3	0 23	$>10^5$
80Ni 20Fe	–	100 000	–	–	0 87	57
84fe-16Al	450	55 000 116000	0 38	1 98 3 20	0 78 0 80	150

Table 1 3 Properties of selected hard magnetic materials[12]

chemical Formula/ composition (wt%)	Curie temperature Tc(^{o}C)	Remanence magnetic induction B_r (Tesla)	Coercive magnetic field H_c (A m^{-1})	Maximum magnetic energy $(BH)_{max}$ kJm^{3}	Demagnetization induction B_d	Electrical resistivity ρ (μΩcm)
BaO $6Fe_2O_3$	450	0 220	145 000	8	0 11	10^{12}
SrO $6Fe_2O_3$	460	0 400	175 000	27	0 185	10^{12}
$BaFe_{12}O_{19}$	450	0 400	160 000	29	—	—
76 7Pt 23 3Co	480	0 645	355 000	74	0 35	28
Fe 52Co 14V	_	700	42000	28	—	—

They possess unique combination of properties of magnetic materials and insulators Table 1 4 summarizes the properties of selected ferrites Their structure can be described by close packed layers of oxygen ions with metal ions occupying tetrahedral and octahedral voids Depending upon the crystal structure ferrites fall into two main groups

Cubic close packed with general formula MFe_2O_4 or MO Fe_2O_4 where M stands for a divalent metal ion like Mn Ni Fe Co Mg etc Among these only cobalt ferrite (Co Fe_2O_4) is hard while all others are soft in nature Soft ferrites are used in computer memory cores television receivers communications radios recording heads, magnetostriction transducers

Table1 4 Properties of selected ferrites

Ferrite type	Chemical formula	Structure type crystal system lattice parameters and space group	Magnetic induction saturation B_s	Curie temperature Tc(°C)
Ba Fe ferrite	$BaFe_{12}O_{19}$	Hexagonal	0 45	430
Cobalt ferrite	$CoFe_2O_4$	Spinel type cubic Fd3m	0 53	520
Copper ferrite	$CuFe_2O_4$	Spinel type cubic Fd3m	0 17	455
Franklinite	$ZnFe_2O_4$	Spinel type cubic (a=0 842 nm) Fd3m	0 50	375
Jacobsite	$MnFe_2O_4$	Spinel type cubic, (a=0 851 nm) Fd3m	0 50	300
Lithium ferrite	$LiFe_5O_8$	Spinel type cubic Fd3m	0 39	670
Magnesioferrite	Mg Fe_2O_4	Spinel type cubic (a=0 838 nm) Fd3m	0 14	440
Magnetite	Fe_3O_4	Spinel type cubic (a=839 4 pm) Γd3m	0 60	585
Ni Al ferrite	$NiAlFe_2O_4$	Spinel type cubic Fd3m	0 05	1860
Nickel ferrite	$NiFe_2O_4$	Spinel type cubic Fd3m	0 34	575

microwave devices etc [11] They have a general formula AB_2X_4 and crystallize into spinel structure which can be visualized in terms of cubic close packed arrangement of anions with one half of the octahedral holes (B sites) and one eighth of the tetrahedral holes (A- sites) filled with cations There are eight of AB_2X_4 formula units in the unit cell with location of ions as under

Equivalent positions (0 0 0 0 ½ ½ ½ 0 ½ ½ ½ 0) +

8A at 0 0 0 ¼ ¼ ¼

16 B at $^5/_8$ $^5/_8$ $^5/_8$ $^5/_8$ $^7/_8$ $^7/_8$ $^7/_8$ $^5/_8$ $^7/_8$ $^7/_8$ $^7/_8$ $^5/_8$

32 O at x x x $^1/_4$ x $^1/_4$ x $^1/_4$ –x,

x $\bar{x}$ $\bar{x}$ $^1/_4$ –x $^1/_4$ +x $^1/_4$ +x,

$\bar{x}$ x $\bar{x}$ $^1/_4$ +x $^1/_4$ x $^1/_4$ +x,

$\bar{x}$ $\bar{x}$ x $^1/_4$ +x $^1/_4$ +x $^1/_4$ x

In the non-ideal structure the anions are moved from their ideal positions in <111> directions and the value of x deviates from 3/8 Fig 1 1 shows the complete unit cell with distribution of A B and oxygen ions together with tetrahedral A site and octahedral B site, respectively Also layer sequence along z direction is depicted at the bottom Fig 1 2 gives schematic view of the spinel structure with two types of octants (I and II) disposed in the unit cell Both octants are depicted separately too with ions

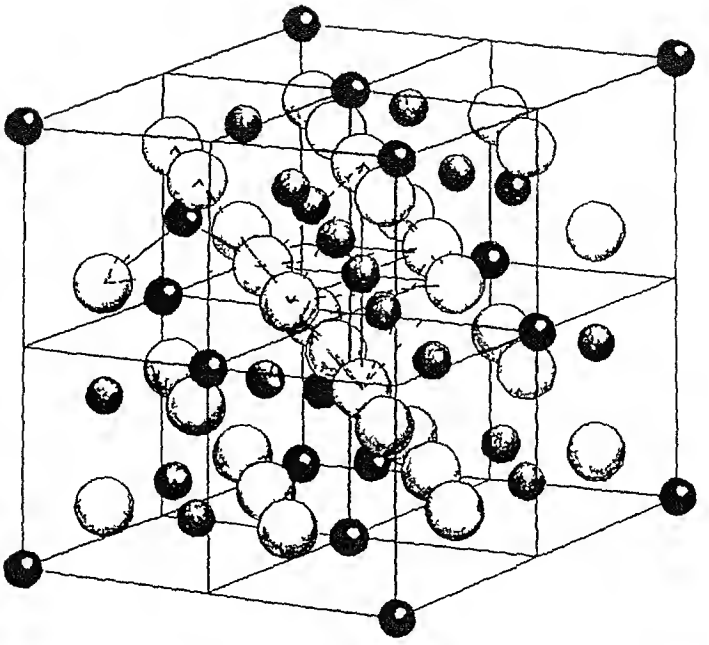

A B O

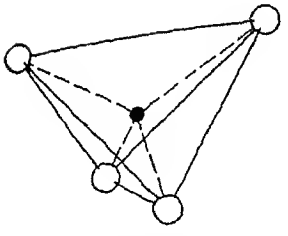

Tetrahedral A site

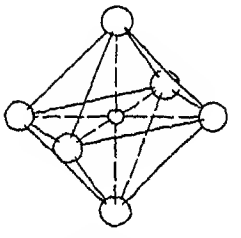

Octahedral B site

Layer sequence-

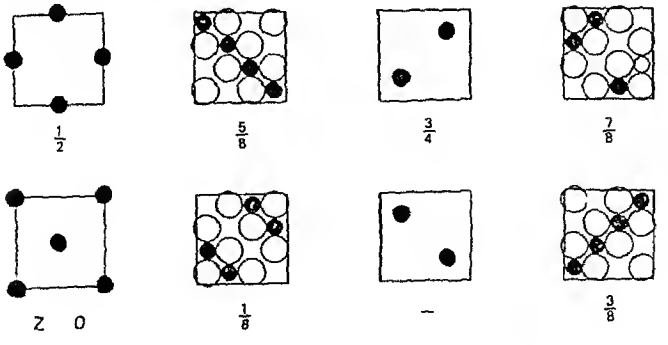

Fig 1 1 The spinel structure

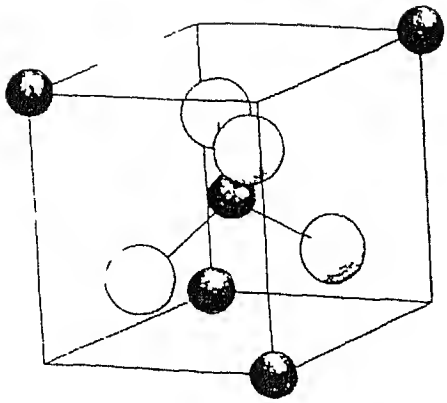

Type I octant containing A cations in tetrahedral co-ordination

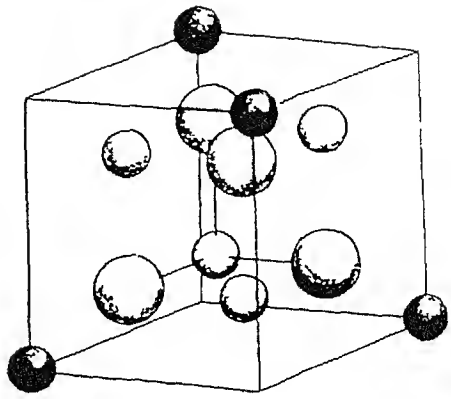

Type II octant containing B cations in octahedral co-ordination (octahedral extent beyond single octant)

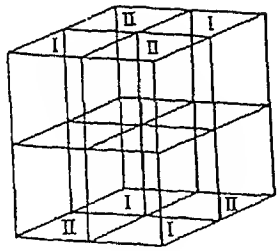

Fig 1 2 The spinel structure

locations There are one A and three B cations around each anion at a(x 1/4)√3 and a(5/8 –x) respectively Also the angles B-X B and A X-B are about 90 and 125 respectively These angles and distances are important in determining the magnetic properties of spinel ferrites There are indirect or super exchange interactions the strongest being between the A ions in tetrahedral sites and B- ions in octahedral sites due to their small separation and large A X-B angle Thus the nature of cation distribution on the two sites is also important for determining the magnetic behaviour

For inverse spinel the formula is rewritten as $B(AB)O_4$ This indicates that the A ions and half of B-ions are in octahedral sites whereas remaining B ions assumes tetrahedral sites

Hexagonal Closed packed with general formula $MFe_{12}O_{19}$ or $MO\ 6Fe_2O_3$ where M represents the large divalent ion such as Ba^{2+} Sr^{2+} or Pb^{2+} They possess low crystal symmetry and so exhibit large magneto crystalline anisotropy The most important in this group is barium ferrite family falling in magnetically hard category [11] The layered structure is shown in Fig 1 3

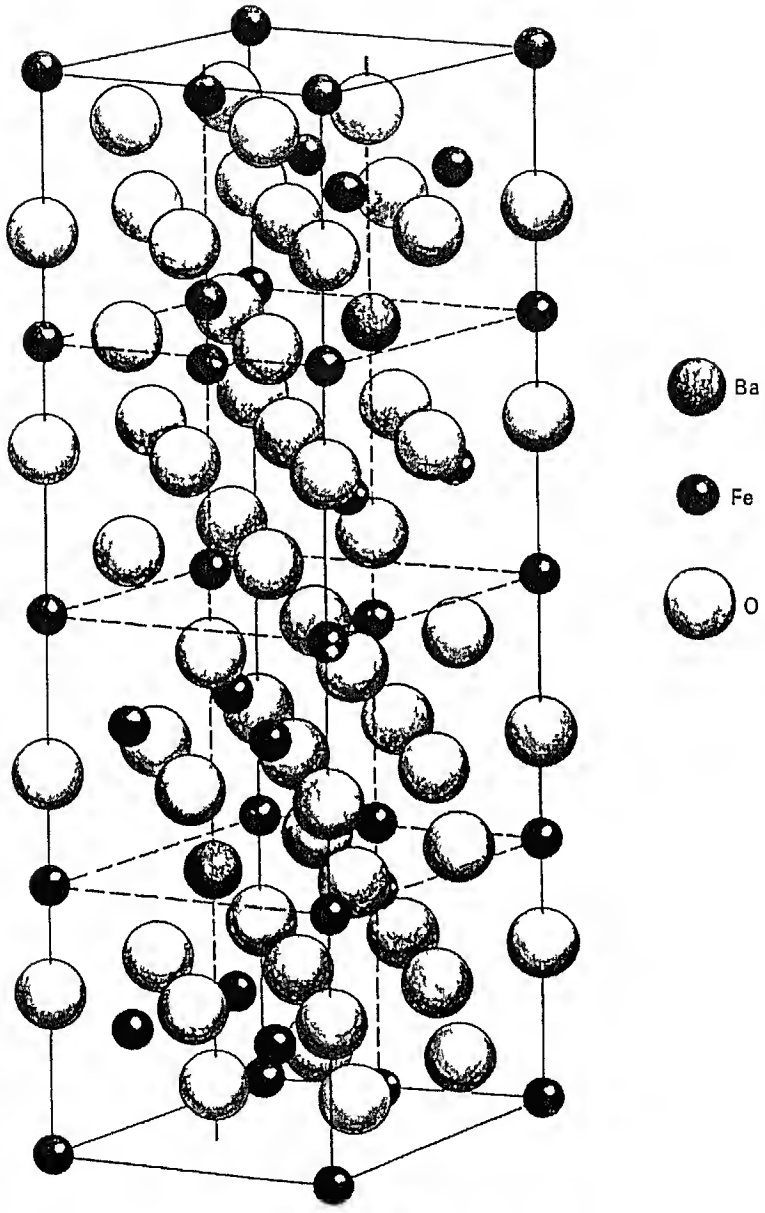

Fig 1 3 The structure of $BaFe_{12}O_{19}$

The physical and chemical properties of spinel ferrite arise from the ability of these compounds to distribute the cations among the available A and B sites Therefore control of cations provide the means to control the magnetic behaviour[9] The so called cation distribution is proved to be an equilibrium function of temperature pressure and composition The magnetic properties of materials depend largely on microstructure which in turn varies with the preparation methods

1 1 Preparation method

Different methods/processes developed for the preparation of ferrite include ceramic solution and co precipitation, hydrothermal synthesis and glass crystallization organometallic precursor route pyrosol and sol gel etc [14] The basic production operations common to all methods consist of mixing of initial components (mechanically or chemically) heat treatment under suitable conditions (i e , temperature, time, environment, etc) and cooling It is possible to obtain a homogeneous powder by adjusting the preparation conditions appropriately [14] Some of the methods used for the synthesis of specific ferrites, superconductors etc are described below However, these may be extended to any system after optimization of the process

1 2 1Cryogenic technology

This method has been used to prepare chemically homogeneous one domain barium ferrite crystallites with high values of saturation magnetization and coercive force [14] It involves preparation of initial aqueous salt solutions of barium and iron nitrates their mixing in proportion as per the stoichiometry desired of the final product and cryocrystallization (i e rapid cooling provided by dispersion of the solution into the liquid nitrogen) The process yields spherical shape particles called cryograins of average diameter (d~3 5 mm) with uniform distribution of salt components The frozen solvent (ice) is removed from cryograins by freeze drying at sufficiently low temperature and pressure to prevent their melting The resulting product (being a hygroscopic powder) is subsequently given a heat treatment at 700 1200^{0}C for 5 min [14]

1 2 2 Gel to crystallite conversion

The reaction basically involves chemical influx of alkovalent ions to generate pressure causing breakdown and direct conversion of gel into crystallites A reactive gel of hydrated ferric hydroxide $Fe(OH)_3\ xH_2O$ ($70<x<110$) is prepared by pouring ammonium hydroxide into ferric chloride solution at 30-40^{0}C and attaining pH in the range of 6 8 It is washed for removal of anions and ammonium ions The gel is suspended in

$Ba(OH)_2$ solution in presence of hydrophilic solvent (e g ethanol) in a flask fitted with a water cooled reflux condenser Air in the vessel is replaced by nitrogen Fresh entry of CO_2 is prevented with an alkali guard tube and the reaction is carried out at 80 95^0C for 4 6 h The solid phase present in the vessel is then filtered washed thoroughly to remove $Ba(OH)_2$ and air dried The resulting product is a nanosized crystallite precursor which on thermal treatment at elevated temperatures yields hexaferrite phase(s) The reaction can be summarized as under

$$12Fe(OH)_3 \; xH\,O(gel) + Ba(OH)_2 \xrightarrow{75\ 90\ C} BFe_{12}O_{15\,71}(OH)_{6\,58}\ 7H\,O$$
$$\xrightarrow{00\ C} BaFe_{12}O_{15\,71}(OH)_{6\,58}(precursor) + 7H_2O$$
$$\xrightarrow{600\ C} BaFe_{12}O_{19}(Hexaferrite) + 3\,29H_2O$$

This is a generally used for preparation of nanosized multinary oxides such as aluminates ferrites zirconates and titanates Also various ferromagnetic oxides possessing structures closely related to hexaferrites can be prepared by partially substituting the Fe^{3+} with divalent / trivalent transition metal ions The main advantage of this process lies in its simplicity operational cost and capacity to produce powders of high surface area with increased homogeneity The product thus exhibits relatively high reactivity and require lower sintering temperature Further the raw materials are not very expensive either [15]

1 2 3 Combustion process

This process saves a lot of time and energy and has been used for synthesis of $YBa_2Cu_3O_7$ superconductor For this stoichiometric amounts of Y_2O_3 and CuO are dissolved in nitric acid and then fine powder of barium nitrate is added Urea powder is subsequently added to form a slurry according to the reaction

$$6M(NO_3) + 5X(NH) CO \rightarrow 5XCO + 10XH_2O + 8XN_2 + 6MO$$

Here M and x represent the metal and its valency respectively When a number of metal nitrates are taken together x is taken as weighted average of the valencies of the constituent metals The slurry mixture is transferred to a glass dish and placed in the furnace at a certain temperature (say 520^0C) The material froths vigorously and ignites with a flame on its own The entire process takes just a few minutes The resulting black powder is heat treated directly or subjected to a second combustion with ammonium nitrate and urea mixture before the heat treatment The second combustion route helps in cutting down the heat treatment requirements [16]

1 2.4 Glass ceramic method

Fine particles of $BaFe_{12-2x}Co_xTi_xO_{19}$ (x=0-0 9) ferrite has been prepared with this method by taking appropriate molar ratio of $BaCO_3$ B_2O_3 and Fe_2O_3 and forming a glass In order to avoid crystallization the

molt is poured between two steel rollers separated by 0 33 mm rotating in opposite directions at angular speed of 80 100 rpm The resulting glass flakes of typical thickness~0 1 mm formed are crystallized at 600^0 1000^0C and immersed in a weak acid subsequently to separate Ba ferrite particles [17]

1 2 5 Chemical coprecipitation and salt induced crystallization

This process has been used for the low cost production of substituted barium ferrite particles of hexagonal and plate like morphology with narrow size distribution,e g $BaFe_{12\ 2x}Co_xTi_xO_{19}$ (x=0-0 9) and $BaFe_{12\ 2x}Co_xSn_xO_{19}$ (x=0 1 4)

An aqueous solutions of the metal chlorides (containing $Ba^{?+}$ Fe^{3+} Co^{2+} and Ti^{4+} or Sn^{4+} in appropriate ratio) NaOH and Na_2CO_3 are mixed and stirred A suspension containing intermediate precipitate is filtered off, washed thoroughly and dried It is then mixed with a pure or mixed salt (like NaCl or NaCl KCl) and heated at appropriate temperature (e g 600-1000^0C) to yield crystalline ferrite particles [17]

1 2 6 Melt coprecipitation and electron beam irradiation

Its characteristic feature is that crystallization takes place not in a liquid phase but in a slightly melted micro regions at a rate usually observed in the solid phase As a result single domain platelet and

hexagonal shaped crystals with mean planar diameters equal to or less than 0 25 μm are produced at temperature above 980^{0}C in just an hour or so Here $BaFe_{10\,4}Co_{0\,8}Ti_{0\,8}O_{19}$ is taken as an example to describe the procedure The initial components viz γ Fe_2O_3 $BaCO_3$ $CaCO_3$ and TiO_4 (ferrite forming in appropriate quantity) and $BaCl_2$ $2H_2O$ and B_2O_3 (flux in proportion of 70 30 wt%) are mixed properly and subjected to melt coprecipitation For increased rate of solid phase reaction via faster diffusion of metal ions 1 2 MeV electron beam is allowed to impingelocally on the mixture The dose is maintained at (0 5 0 6)X10^{13} particles/cm^2 to achieve temperature in the range of 800^0 1000^{0}C

The electron beam spot could be increased upto 5 cm diameter without causing any temperature variation After annealing the cooled frit is treated with the dilute solution of acetic acid at ~80^{0}C for separating the ferrite crystals from the flux matrix [18]

Table 1 5 compares the pure thermal and electron beam irradiation methods It clearly indicates advantage of radiation treatment in terms of lowering of temperature and/or reduction in time

Table 1 5 Synthesis conditions of single domain ferrite crystals of $BaFe_{10.4}Co_{0.8}Ti_{0.8}O_{19}$ by the melt coprecipitation method using pure thermal and electron beam irradiation [18]

Treatment	Specimen	T(°C)	T (min)	Impurity phase αF_2O_3
Radiation (e g , 1 2 MeV electron beam	1	825	60	20
	2	850	60	15
	3	900	30	0
	4	980	15	0
Thermal	5	980	60	0

1 2 7 Hydrolysis of metal organic complexes

Small ferrite particles (e g , $SrFe_{12}O_{19}$) with high coercivity have been prepared successfully by the hydrolysis method of metal organic complexes The advantage of this method lies in the intimate mixing of compositional ions on the atomic scale and easy extraction of small particles because of the precipitates precursor being free from other media

A block diagram outlining the preparation process is given below An ethanol strontium acetylacetonate [$Sr(C_5H_7O_2)_2$ $2H_2O$] or strontium ethoxide [$Sr(C_2H_5O)_2$], and iron acetylacetonate [$Fe(C_5H_7O_2)_3$] or iron ethoxide [$Fe(C_2H_5O)_2$], with appropriate Fe/Sr ratio are stirred in ethanol, refluxed

and hydrolyzed by water By maintaining pH at 12 with an aqueous ammonia solution a hydrated precursor is precipitated and heat treatment at appropriate temperatures to form small particles of $SrFe_{12}O_{19}$ [18]

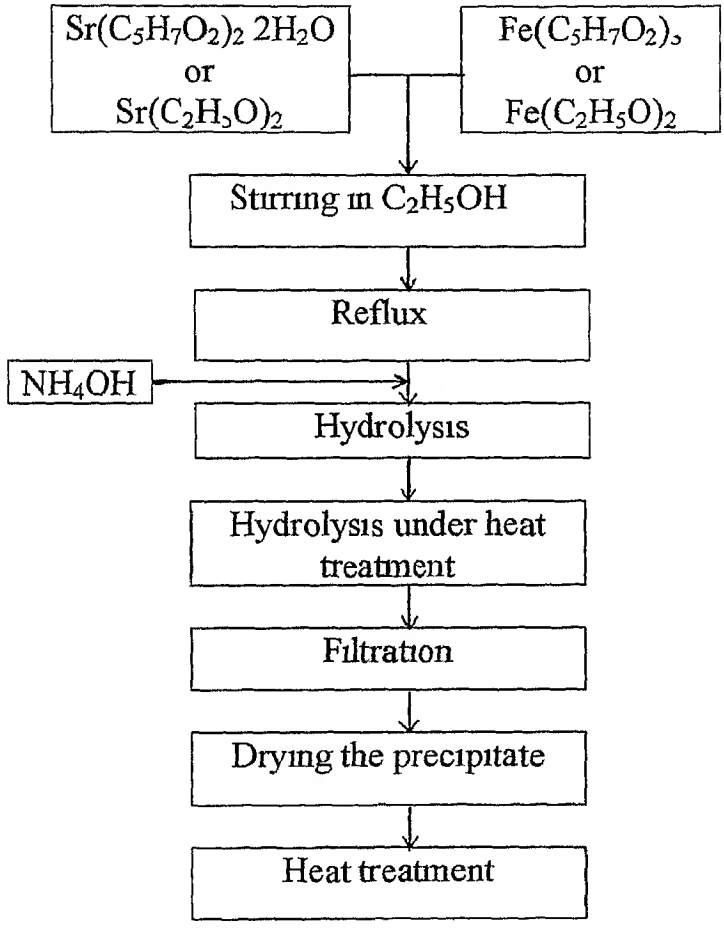

Fig 1 4 Flow chart of hydrolysis of metal organic complex method

1 2 Manganese ferrite system

The magnetic properties of nanoscale have been a subject of interest in the recent past due to increasing microminiaturization and data storage density requirement Also, there is always curiosity to understand the deviation in the properties as bulk is gradually reduced to small dimensions Manganese ferrite $MnFe_2O_4$ is particularly well suited for understanding such studies because of its low Curie temperature (300^0C) This allows examination of ferromagnetic to paramagnetic transitions much before the particles turn superparamagnetic due to thermal effect Nevertheless $MnFe_2O_4$ is considered to be a complex system with regard to variation in its resulting viz , characteristics saturation magnetization coercive field Curie temperature, cation redistribution etc with the synthesis methods adopted and nature of heat treatment followed/imparted The literature review given below reflects the continuing interest on this system as its characteristics are not fully understood

Tang, Sorensen Klabunde, and Hadjipanayis [20] have prepared fine manganese ferrite ($MnFe_2O_4$) particles (diameter~5 25 nm) by co-precipitation of manganous and ferric salts with hydroxide and subsequent digestion process below 100^0C The findings indicate that the particle size strongly depends on the metal ion to hydroxide ion concentration ratio The

undigested samples were found to be polycrystalline with average crystallite size of about 2nm The digestion led to increase of crystallite size to ~5nm via Ostwald ripening process Mossbauer spectrum of the digested sample could be fitted with a sextet and fitting parameter as quadrupole splitting $|\Delta E|$ =0 10(2) mm/s isomer shift δ=0 33(2) and internal magnetic field (H)=466kO Lateron Tang et al [21] also measured magnetization as a function of temperature in a small applied field of 20Oe for $MnFe_2O_4$ and found considerable enhancement in Curie temperature (Tc) with decrease in size of nanoscale particles in the range of 7 5 24 4 nm For example in particles of size 7 5 nm Tc was 97K higher than for the bulk material Such a shift in Tc was described by the finite size scaling,formula

$[Tc(d) Tc(\infty)]/Tc(\infty)=+(d/d_0)^{1/v}$ with exponent v=0 71±0 07 characteristic microscopic dimension parameter (d_0)=2 0 nm and $Tc(\infty)$=573K However in subsequent studies[23] such an increase in T_c was attributed to the variation caused in degree of inversion of the spinel structure due to $Mn^{2+} \rightarrow Mn^{3+}$ conversion as a function of particle size Nevertheless particle of size ~5 nm were reported to exhibit superparamagnetism[20]

Zheng Wu Zon and Wang [22] have synthesized nanosized $MnFe_2O_4$ particle by chemical ultrasonic emulsion method which essentially involves mixing of aqueous solutions of Mn^{2+} and Fe^{3+} nitride

salts and dodocal benzene sulfuric acid sodium salt (DBS) adding appropriate amount of toluene generating microemulsion under continuous stirring subjecting to ultrasonic and finally adding appropriate amount of NaOH to get a sol By washing and distilling, DBS coated $MnFe_2O_4$ nanoparticles were obtained The samples were also annealed at 400^0C in vacuum ~ $5x10^{-4}$ Pa for 1 h This led to creation of ferromagnetic spherical particles of mean size ~ 5 6 nm with a low saturation magnetization (σ_s) value of 24 4 emu/g compared to bulk (σ_s being 80 emu/g) The reduced saturation magnetization was attributed to the presence of magnetic dead layer of thickness~0 6 nm on the surface of the particle an approach adopted earlier too [21 23] The saturation magnetization versus temperature plot in the range of 300 1173 K reveals Curie temperature (Tc) as 733 K a value 160 K higher than the corresponding bulk value It is believed that enhancement of Tc results due to contributions from both finite size effect [20] and cation redistribution on tetrahedral and octahedral sites

Ding, McCormick and street [24] have reported formation of nanocrystalline $MnFe_2O_4$ of average particle size ~ 35 40 nm with saturation magnetization of 54 79 emu/g by mechanical alloying of Mn_2O_3 and Fe_2O_3 in the hardened steel vial using 12 mm diameter steel balls for 66 h or longer under an argon atmosphere and subsequent annealing at 700^0C in vacuum

Further addition of manganese is found to accelerate the formation process of $MnFe_2O_4$

Mohamoud Williams Cai Siu and Walker [25] formed polycrystalline films of manganese ferrite by pulse laser deposition onto glass at substrate temperatures of 200 550^{0}C While the stoichiometry remained intact in the film cation distribution was found to be very different from the source target

Nanosized $MnFe_2O_4$ particles with mean diameter of 9 nm have been synthesized by thermal deposition of a manganese iron citrate precursor at 623 K in an inert atmosphere [26] Their saturation magnetization value of 53 emu/g at 5K (bulk value~110emu/g) was attributed to incomplete alignment of spins or presence of magnetic dead layer of 0 6 nm thickness at the surface of particles Magnetization-temperature curve at a field of 100 Oe depicted two peaks at 125 – 150K and 21K arising due to super magnetic blocking and surface freezing of moments respectively

Kulkarni Kannam Arunarkavalli and Rao [27] prepared $MnFe_2O_4$ by coprecipitation method [21] but annealed in helium at 773 K for 1 h and cooled slowly to room temperature for ensuring equilibrium cation distribution Their ^{57}Fe Mossbauer spectra exhibit sextet and could be fitted with values of isometric shift of 0 4 mms^{-1} and internal magnetic field of 463

kOe Also an increase of Curie temperature (Tc) by 50 K (from bulk value of 573 K) observed in particles of average size ~12 nm was attributed to finite size scaling

Upadhyay Davies Wells and Cherles [28] have evaluated magnetic properties and size distribution parameter of ultrafine particles of $MnFe_2O_4$ and $Mn_{1-x}Fe_xFe_2O_4$ ($x \leq 0.9$) They observed (a) decrease of particle size from 11.3 to 6.7 nm with increase of manganese content from x = 0.1 to 0.9 (b) a constant reduced remanence (M_r/M_s) of 0.4 at 4K (a value smaller than that estimated for random distribution of uniaxial particles) and attributed to flux closure and spin pinning (c) lowering of blocking temperature (corresponding to peak in susceptibility vs temperature plot) with increase in manganese content, caused by decrease of both particle particle interactions and effective anisotropy constant and (d) superparamagnetism behavior viz no hysteresis and superposition of magnetization versus (H/T) curves

Rath Sahu Anand Date Mishra and Das [29] synthesized nanosize (9-12 nm) $Mn_{0.65}Zn_{0.35}Fe_2O_4$ particles from metal chloride solution through a hydrothermal precipitation route using aqueous ammonia at pH~10 and reported both the Curie temperature (Tc) and coercivity (Hc) to be high as compared to the bulk values

Lopez Pfannes Paniago Tourinho [30] studied $MnFe_2O_4$ nanoparticles of average size 6-9 nm by Mossbauer spectroscopy and estimated cation distribution as $[Mn_{0.1}Fe_{0.9}][Mn_{0.9}Fe_{1.1}]O_4$ i e concentration of Mn^{2+} ions in B-sites is close to that of an inverse spinel

1 3 Objective of present work

The objective has been to study the effect of partial substitution of manganese with zinc in $MnFe_2O_4$ For this compounds of compositions $Mn_{1-x}Zn_xFe_2O_4$ (x=0 0 2 0 3 0 4 and 0 5) have been prepared by co precipitation and characterized with regard to their phase(s) morphology surface area and magnetic properties (viz saturation magnetization and Curie temperature hysteresis loop etc) by employing X-ray powder diffractometer transmission electron microscope BET surface area analyzer and vibrating sample magnetometer

Chapter 2

2 1 Experimental Details

In this chapter, the experimental details pertaining to synthesis of pure and modified manganese ferrite by partial substitution of Mn^{2+} and their characterization by X-ray powder diffractometer transmission electron microscope BET surface area analyzer and vibrating sample magnetometer as given

2 1 1 Synthesis of manganese ferrite ($MnFe_2O_4$)

The raw materials used are listed in Table 2 1 with manufacturer and purity The synthesis of $MnFe_2O_4$ is carried out by co precipitation method. Initially solutions of the sodium hydroxide (NaOH) and the metal Fe(3+) and Mn(2+) salts are prepared in distilled water For this 6 00 g of NaOH is dissolved in 100 ml of distilled water Also 2 70 g of $FeCl_3$ $6H_2O$ and 0 99 g of $MnCl_2$ $4H_2O$ are dissolved in 50 ml of water separately The atomic ratio of Mn(2+) to Fe(3+) thus becomes 0 5 The metal salts solution is then poured in the sodium hydroxide solution mixed well using a magnetic stirrer and brought to a pre-heated bath of water and ethylene glycol for precipitation and digestion The temperature is maintained at 90^0C for about 90 minutes Stirring is continued during the digestion process Suspension is repeatedly washed with water filtered and dried at 50^0C for 7-8 h to yield a product as a powder

For synthesis of manganese ferrite of composition $Mn_{1-x}Zn_xFe_2O_4$ with x=0 2 0 3 0 4 and 0 5 besides $MnCl_2\,4H_2O$ and $FeCl_3\,6H_2O$ appropriate amount of $ZnCl_2$ is dissolved in water The resulting salt solution is then poured in sodium hydroxide solution mixed well using a magnetic stirrer and digested at 90°Cfor 90 minutes, as before The precipitate is rapidly washed with water filtered and dried at 50°C for 7-8 h The resulting powder is calcined at 200°Cfor 2h to get the final product

Table 2 1 List of raw materials used for synthesis

Materials	Manufacturer	% Purity
Manganese chloride $MnCl_2\,4H_2O$	Polypharm Private Limited	95
Ferric chloride $FeCl_3\,6H_2O$	Ranbaxy Lab Ltd	96
Sodium Hydroxide NaOH	Qualigens fine chemical	98
Zinc Chloride $ZnCl_2$	E Merck (India) limited	95
Ethylene Glycol	Ranbaxy Pvt Ltd	95

2 2 Characterization techniques

2 2 1 X-ray diffraction (XRD)

The XRD pattern of powder samples have been recorded in a X ray diffractometer (Rick Seifert model ISO Debye flux 2002) using a CuKα radiation to ascertain their nature and determine the phase(s) present For this powder was packed in a 10 mm diameter circular cavity of aluminum holder which in turn was mounted in its position on the sample stage of the diffractometer The diffracted beam was received by a scintillation counter detector held at an angle of 2θ with the transmitted beam (θ being the angle between the sample surface and the incident beam) The rotation movement of the sample and the detector was synchronized such that the incident and diffracted beams always made the same angle (θ) with the sample surface The X ray tube was operated at 30 kV and 20 mA and diffraction pattern recorded at a scanning rate of 3^0/min in the range of 25-100^0 The time constant was set at 10 seconds and sensitivity was either 5000 or 2000 counts per minutes The XRD pattern was continuously observed on the monitor of a personal computer and finally printed

2 2 2 TEM Studies

Manganese ferrite ($MnFe_2O_4$) and zinc substituted manganese ferrite ($Mn_{1-x}Zn_xFe_2O_4$) have been observed in a transmission electron microscope (JEOL JEM 2000 FX) for their microstructure phase(s) and crystallographic orientations For this support film was first prepared on glass substrate using formvar solution in chloroform (0 4 g/100ml) and then allowed to float on water surface This was subsequently transferred onto the matt side of copper specimen grid Ferrite powder was crushed and dispersed in isobutyl alcohol by shaking well and allowed to settle for sometime A few drops of suspension were then placed on the formvar coated grid with the help of a micropipette On drying up the samples were stored and/or transferred to the TEM for examination The microscope was operated at 120kV The micrographs and selected area diffraction patterns were recorded from different regions on a 35 mm film

2 2 3 Surface area measurement

The BET (Brunauer Emmet and Teller) method is commonly used for measuring specific surface area (which include internal area as well) It is based on physical absorption process where known gas molecules (say of nitrogen) are condensed onto the sample surface as a monolayer and

the resultant pressure in the closed chamber is measured The pressure data when monitored at a constant temperature allows construction of an isotherm which in turn can be used to extract total internal surface area

The BET function varies linearly and often represented as

$$\text{BET function} = \frac{P}{V_1(P-P)} = \frac{1}{V_M C} + \left[\frac{C-1}{V_M C}\right] X \left(\frac{P_S}{P_O}\right)$$

where V_m = volume of monolayer P_S is sample pressure V_A is volume adsorbed P_o is saturation pressure C is constant related to the enthalpy of adsorption With a specific pressure range (usually 0 05 to 0 2 atm) an isotherm is obtained and used to calculate the BET function Its plot is then made against relative pressure (P_s/ P_o) and linearly fitted to get values of slope (C-1)/ V_MC and intercept 1/ V_MC The BET surface area in (m^2/g) is then determined from the following expression

$$S_{BET} = \frac{V_M N_A A_M}{M_V}$$

where S_{BET} is the BET surface area N_A is Avogadro number A_M is the cross-sectional area occupied by each adsorbate molecule and M_V is the gram molecular volume (22414 m^2) For nitrogen the value of A_M is assumed to be 0 162nm^2

The samples were prepared by grinding the powder thoroughly in an agate mortar The surface area was measured using the Coulter SA 3100 analyzer and nitrogen as the gas for adsorption

2 2 4 Magnetic measurements

A pellet of size 3mmx3mmx2mm was made by using a special die (fabricated for the purpose) at a pressure of~2×10^5KN/m^2 The pellet was weighed and introduced in the vibrating sample magnetometer (Princeton VSM Model 150A) equipped with an electromagnet (Varian model V 2700) capable of providing a maximum magnetic field of ~ 11 5 kOe

The magnetic moment measurements were also made as a function of temperature at a fixed magnetic field of 5000 or 500 Oe to determine the Curie temperature of the products The sample temperature was set with a controller (Indotherm model 401) A regulated power supply (Networks model NPS 30/5D) was used to provide power to the furnace surrounding the sample and the chamber was evacuated using a HHV pumping model A chromel alumel thermocouple was held close to the sample to indicate the temperature

The information gathered includes specific magnetization (M_s) remanence magnetization (M_r), coercive field (H_c) and the Curie temperature (T_c)

The working principle of magnetic moment measurement is described below

When a sample is placed in a uniform magnetic field a dipole moment proportional to the product of its susceptibility and the applied field gets induced Upon subjecting the sample to sinusoidal motion as well an electrical signal is observed in suitably located stationary pick up coils This electrical signal (being at the vibration frequency of the sample) is proportional to the magnetic moment vibration amplitude and vibration frequency For this the pellet is introduced in a sample holder which in turn is centred in the region between the pole pieces of an electromagnet (Fig 2 1) A slender vertical rod connects the sample holder with a transducer assembly located above the magnet The transducer converts a sinusoidal ac drive signal (provided by an oscillator/amplifier circuit located in the console) into a sinusoidal vertical vibration of the sample rod and the sample is thus made to "undergo a sinusoidal motion" in a uniform magnetic field Coils mounted on the pole pieces of the magnet pick up the signal resulting from the sample motion This ac signal at the vibration frequency is in fact proportional to the magnitude of the moment induced in the sample For its detection and measurement an ingenious milling technique is employed Use is made of a vibrating capacitor to generate another

"comparison" signal which varies with moment vibration amplitude and vibration frequency in the same manner as does the signal in the pickup coils By appropriately processing these two signals the effects of vibration amplitude and frequency shifts are cancelled and readings are obtained which vary only with moment the quantity of interest The signal from the pickup points is applied to one input of a differential amplifier The other input signal to the amplifier is derived from the fixed plate assembly of a vibrating capacitor mounted beneath the transducer assembly Applied to the moving plate assembly of the capacitor is a dc voltage proportional to the magnetic moment of the sample Thus an ac signal is coupled onto the fixed plate assembly of the vibrating capacitor and from there to the second input of the differential amplifier Since the dc voltage applied to the moving assembly is proportional to the magnetic moment the signal generated is also proportional to the moment Moreover as the capacitor and the sample are also vibrated by the same transducer as the capacitor output signal varies with changes in frequency and vibration amplitude in the same manner as does the signal from the pickup coils In other words changes in vibration amplitude and frequency have identically the same effect on both of the signals applied to the differential amplifier Since the differential amplifier passes only the differences between the two signals the effects of vibration

amplitude and frequency changes are canceled Thus three factors viz moment vibration amplitude vibration frequency though affect the amplitude of the pickup coil signal only the moment determines the amplitude of the signal at the output of the differential amplifier The signal in turn is applied to a synchronous detector for comparison with a reference signal taken from the same oscillator which furnishes the transducer drive signal At the output of the synchronous detector is a dc signal proportional to the amplitude of the moment This dc signal is amplified and then used in two different ways First it is fed back to the movable plate assembly of the vibrating capacitor Second it is applied to the output display circuits The effect of feedback is to automatically adjust the dc signal to the level required to maintain the capacitor output signal at the same level as the pickup coil signal For samples having small or large magnetic moment the feedback dc voltage will be low or high In any case it will always be proportional to the dipole moment of the sample and independent of variations in the vibration amplitude or frequency As the dc voltage also serves as the input to the display circuitry the output indicates moment magnitude alone uninfluenced by vibration amplitude changes and frequency drift

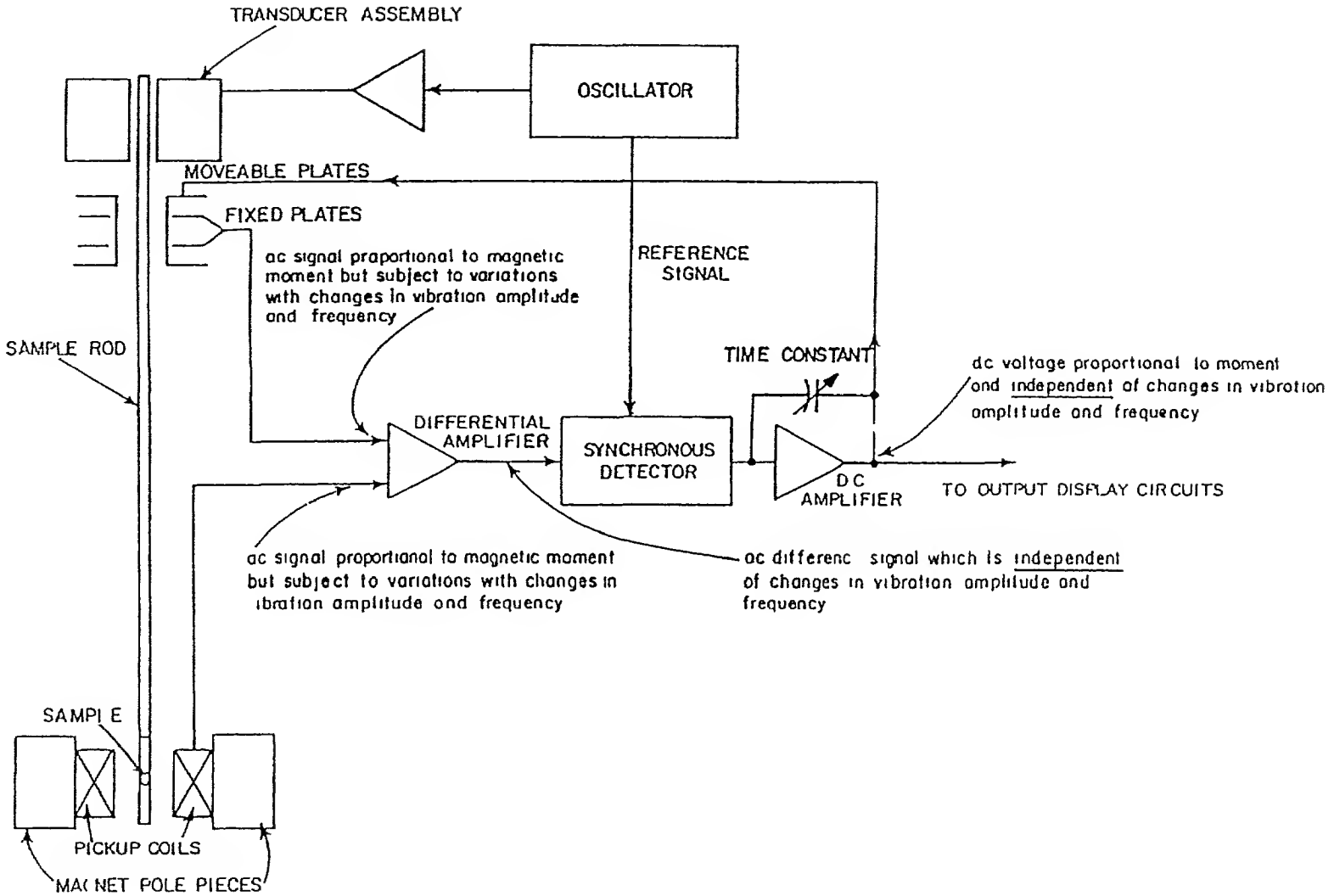

Fig 2 1 Simplified block diagram of magnetometer

Chapter 3

3 Results and discussions

3 1 Phase evaluation

XRD pattern of pure manganese ferrite sample together with a standard aluminum sample recorded with CuKα radiation is shown in Fig 3 1 The diffraction peaks of aluminum are marked and used as a reference to determine the correct 2θ values for diffraction peaks of ferrite samples The 2θ values interplanar (d) spacings and relative intensities of various diffraction peaks with their respective indices are given in Table 3 1 The indexing of pattern suggests a face centred cubic structure for manganese ferrite with a=8 503±0 001 Å Z=8 and space group Fd3m This matches reasonably well with known crystal data of $MnFe_2O_4$ i e lattice parameter a=8 499 Å [33]

XRD patterns for the products of composition $Mn_{1-x}Zn_xFe_2O_4$ with x=0 2, 0 3 0 4 and 0 5 prepared by coprecipitation method and digested at 90^0C for 90 min were recorded similarly with CuKα radiation and using aluminum as a reference (Fig3 1) XRD patterns of pure and zinc substituted manganese ferrite after further calcination at 200^0C for 2 h are depicted in Fig 3 2 Fig 3 3 shows XRD patterns of

$Mn_{1-x}Zn_xFe_2O_4$ with x=0 2 digested at 90^0C for 90 min before and after calcination at 200^0C for 2 h Their comparison reveals that calcination at 200^0C for 2 h yields a better crystalline phase Similarly Figs 3 4 3 5 and 3 6 show XRD patterns for $Mn_{1-x}Zn_xFe_2O_4$ for x=0 3 0 4 and 0 5, respectively Tables 3 2 – 3 5 list 2θ values interplanar (d) spacings and relative intensities of various diffraction peaks with their respective indices for the four compositions The indexing of XRD patterns suggests that the compound $Mn_{1-x}Zn_xFe_2O_4$ continues to maintain an f c c structure But the lattice parameter decreases with increase in zinc content from 8 503 Å to 8 419 Å for x=0 to x=0 5 As Zn^{2+} has small ionic radius (0 83 Å) than Mn^{2+} (0 91 Å) some decrease is expected in the lattice parameter with the improvement in the degree of manganese substitution or increase in zinc content This finding is consistent with the observation of Rezlescu, Sachelarie Popa and Rezlescu[31] who reported increase of lattice parameters in $Ca_xNi_{0.5-x}Zn_{0.5}Fe_2O_4$ with partial substitution (x=0 25) of Ni^{2+} with Ca^{2+} The lattice parameters are reported as 8 390 Å and 8 437 Å for composition having x=0 and 0 25 respectively The ionic radii of Ni^{2+} and Ca^{2+} being 0 78Å and 1 06 Å, respectively [31]

Table 3 1 2θ's, interplanar spacings and intensities of various peaks observed in XRD of manganese ferrite $Mn_{1-x}Zn_xFe_2O_4$, x=0

S No	2θ (°)	Relative intensity	d value (Å)	hkl	Known data [33]		
					2θ (°)	Relative intensity	d value (Å)
1	29 60	32	3 018	220	29 73	35	3 005
2	34 94	100	2 568	311	35 01	100	2 563
3	42 58	16	2 123	400	42 56	25	2 124
4	52 93	12	1 730	422	52 79	20	1 734
5	56 18	40	1 637	511	56 25	35	1 635
6	61 76	51	1 502	440	61 71	40	1 503
7	72 97	10	1 296	533	72 99	20	1 296
8	88 33	12	1 106	731	88 35	30	1 106

Table 3 2(a) 2θ's, interplanar spacings and intensities of various peaks observed in XRD of manganese ferrite $Mn_{1-x}Zn_xFe_2O_4$, x=0 2 ((digested at 90°C for 90 min)

S No	2θ (°)	Relative intensity	d value (Å)	hkl	Known data of $MnFe_2O_4$ [32]		
					2θ (°)	Relative intensity	d value (A)
1	29 89	43	2 989	220	29 73	35	3 005
2	35 23	100	2 547	311	35 01	100	2 563
3	42 58	29	2 123	400	42 56	25	2 124
4	53 22	22	1 721	422	52 79	20	1 734
5	56 75	37	1 622	511	56 25	35	1 634
6	62 04	55	1 496	440	61 71	40	1 503
7	73 82	16	1 283	533	72 99	20	1 296
				731	88 35	30	1 106

Table 3 3(a) 2θ's, interplanar spacings and intensities of various peaks observed in XRD of manganese ferrite $Mn_{1-x}Zn_xFe_2O_4$, x=0 3, (digested at 90°C for 90 min)

S No	2θ (°)	Relative intensity	d value (Å)	Hkl	Known data of $MnFe_2O_4$ [33]		
					2θ ( )	Relative intensity	d value (Å)
1	29 89	47	2 989	220	29 73	35	3 005
2	35 49	100	2 529	311	35 01	100	2 563
3	42 58	26	2 123	400	42 56	25	2 124
4	53 22	15	1 721	422	52 79	20	1 734
5	56 75	38	1 622	511	56 25	35	1 635
6	62 04	57	1 496	440	61 71	40	1 503
7	73 82	16	1 283	533	72 99	20	1 296
8	89 19	17	1 098	731	88 35	30	1 106

Table 3 4(a) 2θ's, interplanar spacings and intensities of various peaks observed in XRD of manganese ferrite $Mn_{1-x}Zn_xFe_2O_4$, x=0 4, (digested at 90°C for 90 min)

S No	2θ (°)	Relative intensity	d value (Å)	hkl	Known data of $MnFe_2O_4$ [33]		
					2θ (°)	Relative intensity	d value (Å)
1	30 15	49	2 964	220	29 73	35	3 005
2	35 52	100	2 527	311	35 01	100	2 563
3	42 58	42	2 123	400	42 56	25	2 124
4	53 22	24	1 721	422	52 79	20	1 734
5	56 75	48	1 622	511	56 25	35	1 635
6	62 71	66	1 481	440	61 71	40	1 503
7	74 01	15	1 281	533	72 99	20	1 296
8	89 61	19	1 094	731	88 35	30	1 106

Table 3 5(a) 2θ's, interplanar spacings and intensities of various peaks observed in XRD of manganese ferrite $Mn_{1-x}Zn_xFe_2O_4$, x=0 5, (digested at 90°C for 90 min)

S No	2θ (°)	Relative intensity	d value (A)	hkl	Known data of $MnFe_2O_4$ [33]		
					2θ (°)	Relative intensity	d value (Å)
1				220	29 73	35	3 005
2	35 80	100	2 558	311	35 01	100	2 563
3	42 86	28	2 110	400	42 56	25	2 124
4	53 22	23	1 721	422	52 79	20	1 734
5	57 03	45	1 615	511	56 25	35	1 635
6	62 33	68	1 489	440	61 71	40	1 503
7				533	72 99	20	1 296
8	89 05	23	1 099	731	88 35	30	1 106

Table 3 2(b) 2θ's, interplanar spacings and intensities of various peaks observed in XRD of manganese ferrite $Mn_{1-x}Zn_xFe_2O_4$, x=0 2 (digested at 90°C for 90 min and calcined at 200°C for 2 h)

S No	2θ (°)	Relative intensity	d value (A)	hkl	Known data of $MnFe_2O_4$ [33]		
					2θ ( )	Relative intensity	d value (A)
1	29 89	44	2 989	220	29 73	35	3 005
2	35 23	100	2 547	311	35 01	100	2 563
3	42 58	25	2 123	400	42 56	25	2 124
4	53 22	17	1 721	422	52 79	20	1 734
5	56 75	37	1 622	511	56 25	35	1 635
6	62 04	53	1 496	440	61 71	40	1 503
7	73 82	18	1 283	533	72 99	20	1 296
8	88 90	18	1 101	731	88 35	30	1 106

Table 3 3(b) 2θ's, interplanar spacings and intensities of various peaks observed in XRD of manganese ferrite $Mn_{1-x}Zn_xFe_2O_4$, x=0 3 (digested at 90°C for 90 min and calcined at 200°C for 2 h)

S No	2θ (°)	Relative intensity	d value (Å)	hkl	Known data of $MnFe_2O_4$ [33]		
					2θ (°)	Relative intensity	d value (A)
1	29 89	58	2 989	220	29 73	35	3 005
2	35 49	100	2 529	311	35 01	100	2 563
3	42 58	31	2 123	400	42 56	25	2 124
4	53 22	23	1 721	422	52 79	20	1 734
5	56 75	46	1 622	511	56 25	35	1 635
6	62 04	77	1 496	440	61 71	40	1 503
7	73 82	23	1 283	533	72 99	20	1 296
8	89 19	31	1 089	731	88 35	30	1 106

Table 3 4(b) 2θ's, interplanar spacings and intensities of various peaks observed in XRD of manganese ferrite $Mn_{1-x}Zn_xFe_2O_4$, x=0 4 (digested at 90°C for 90 min and calcined at 200°C for 2 h)

S No	2θ (°)	Relative intensity	d value (Å)	hkl	Known data of $MnFe_2O_4$ [33]		
					2θ ( )	Relative intensity	d value (A)
1	30 15	37	2 964	220	29 73	35	3 005
2	35 52	100	2 527	311	35 01	100	2 563
3	42 58	25	2 123	400	42 56	25	2 124
4	53 22	13	1 721	422	52 79	20	1 734
5	56 75	13	1 622	511	56 25	35	1 635
6	62 71	51	1 481	440	61 71	40	1 503
7				533	72 99	20	1 296
8	89 61	15	1 094	731	88 35	30	1 106

Table 3 5(b) 2θ's, interplanar spacings and intensities of various peaks observed in XRD of manganese ferrite $Mn_{1-x}Zn_xFe_2O_4$, x=0 5 (digested at 90°C for 90 min and calcined at 200°C for 2 h)

S No	2θ (°)	Relative intensity	d value (Å)	hkl	Known data of $MnFe_2O_4$ [33]		
					2θ (°)	Relative intensity	d value (Å)
1				220	29 73	35	3 005
2	35 80	100	2 558	311	35 01	100	2 563
3	42 86	33	2 110	400	42 56	25	2 124
4	53 22	11	1 721	422	52 79	20	1 734
5	57 03	30	1 615	511	56 25	35	1 635
6	62 33	47	1 489	440	61 71	40	1 503
7				533	72 99	20	1 296
8	89 05	17	1 099	731	88 35	30	1 106

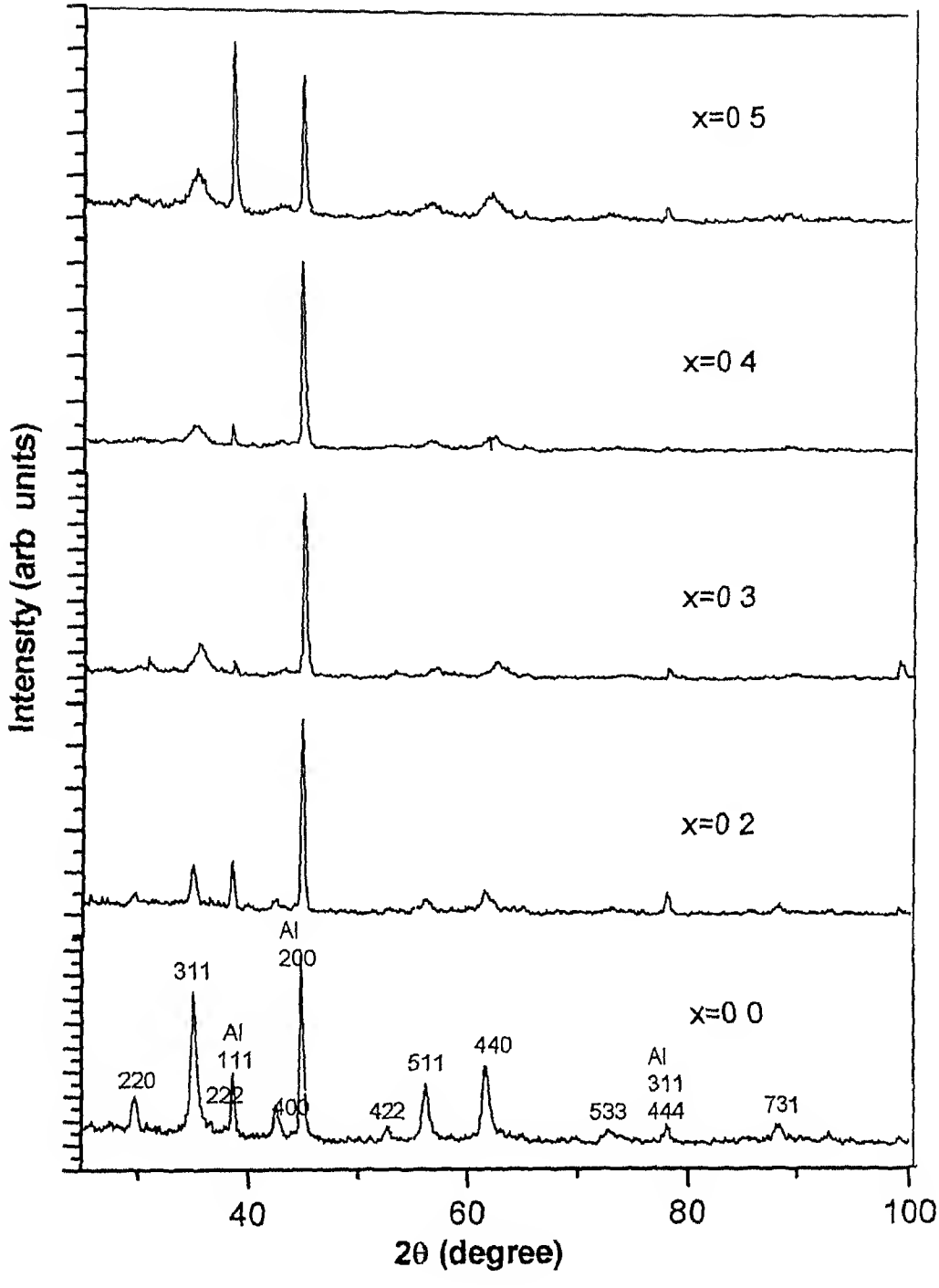

Fig 3 1 XRD patterns of $Mn_{1-x}Zn_xFe_2O_4$ (x=0 0 2, 0 3 0 4 and 0 5) after digestion at 90^0C for 90 min

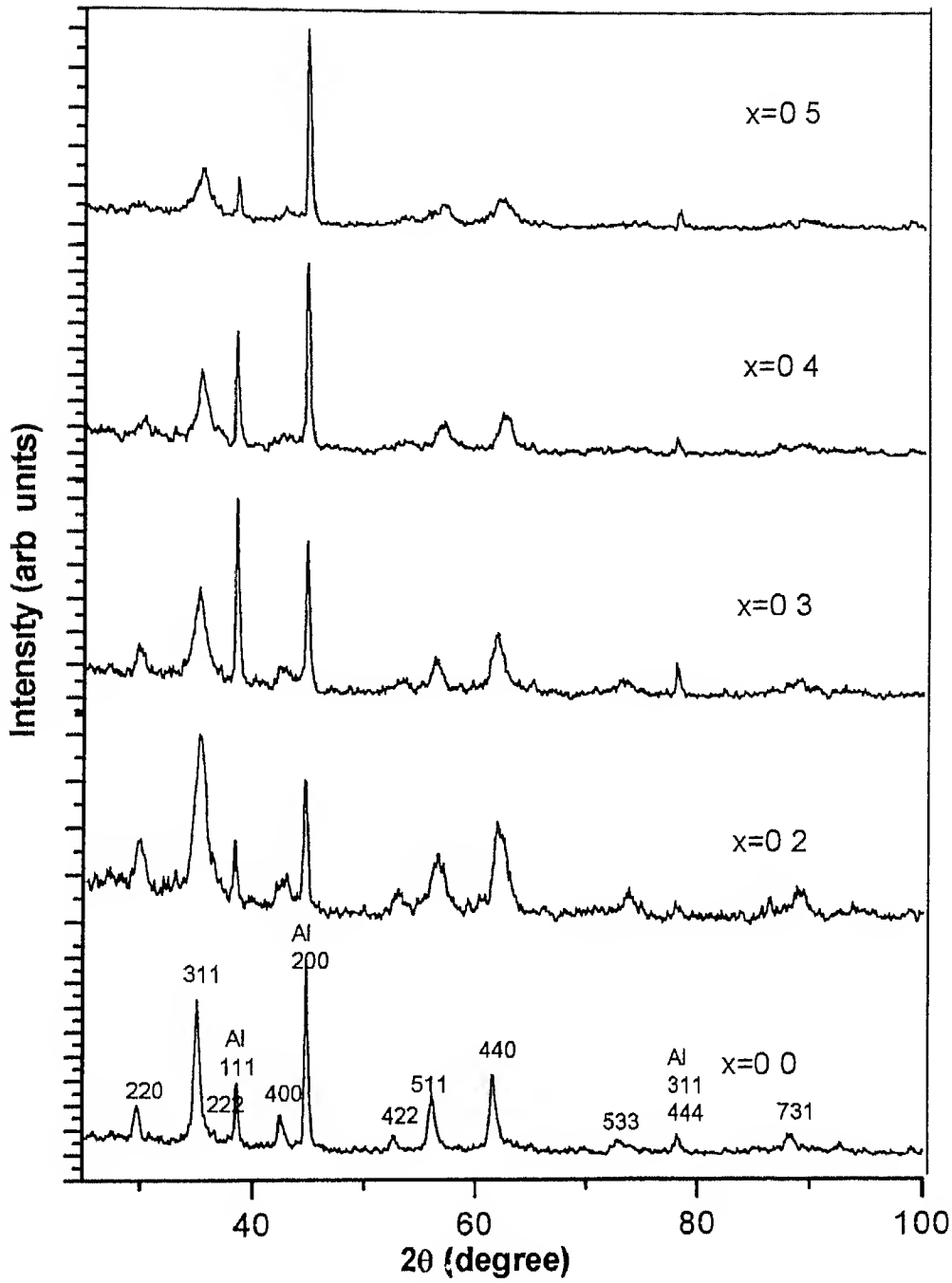

Fig 3 2 XRD patternsof pure $MnFe_2O_4$ prepared by coprecipitation and subsequent digestion at 90^0C for 90 min and $Mn_{1-x}Zn_xFe_2O_4$ (x= 0 2 0 3 0 4 and 0 5) after digestion at 90^0C for 90 min and calcination at 200^0C for 2 h

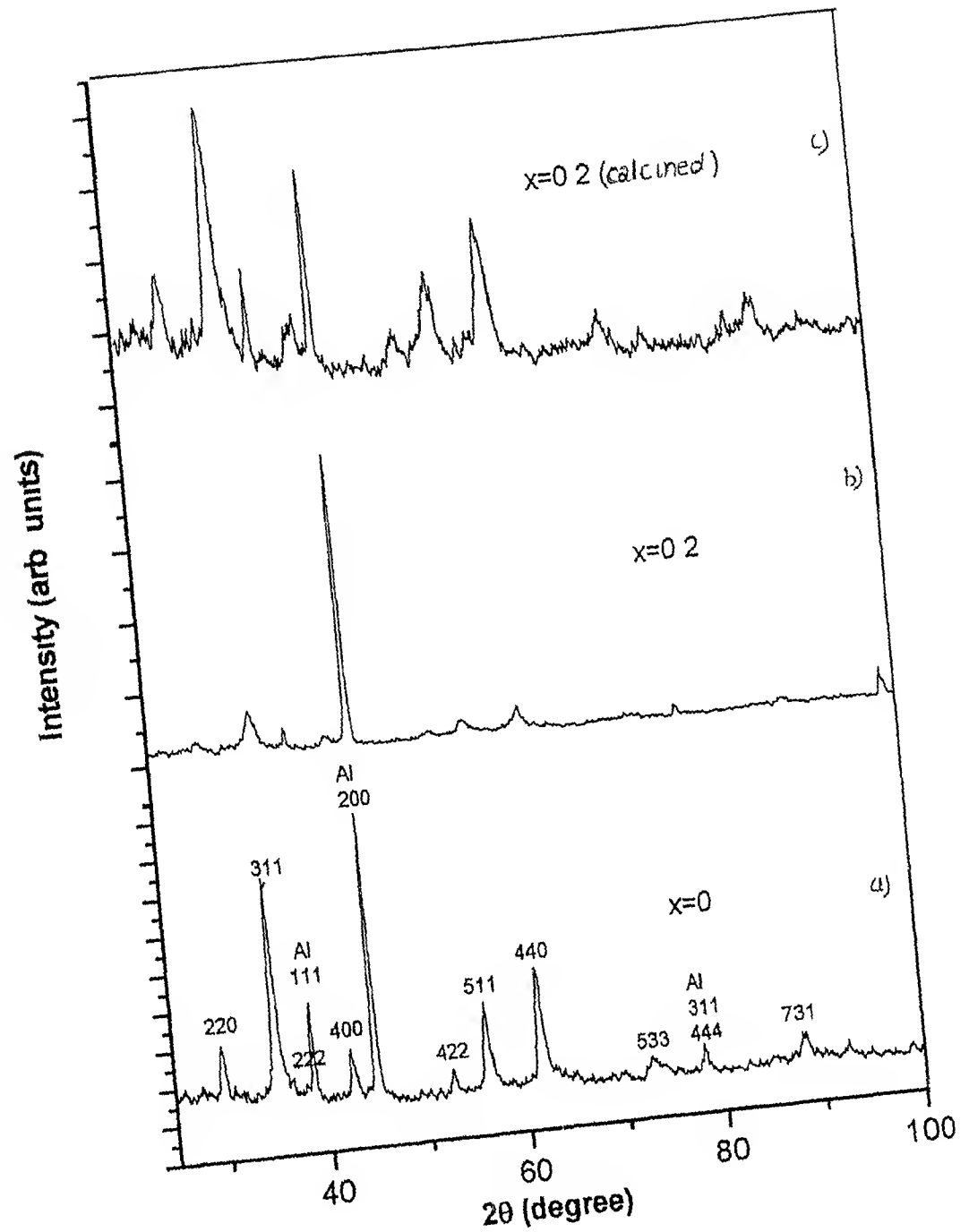

Fig 3 3 XRD pattern of a) pure $MnFe_2O_4$,b) $Mn_{1-x}Zn_xFe_2O_4$,x=0 2 after digestion at 90^{0}C for 90 min and c) $Mn_{1-x}Zn_xFe_2O_4$,x=0 2 after digestion at 90^{0}C for 90 min and calcination at 200^{0}C for 2h

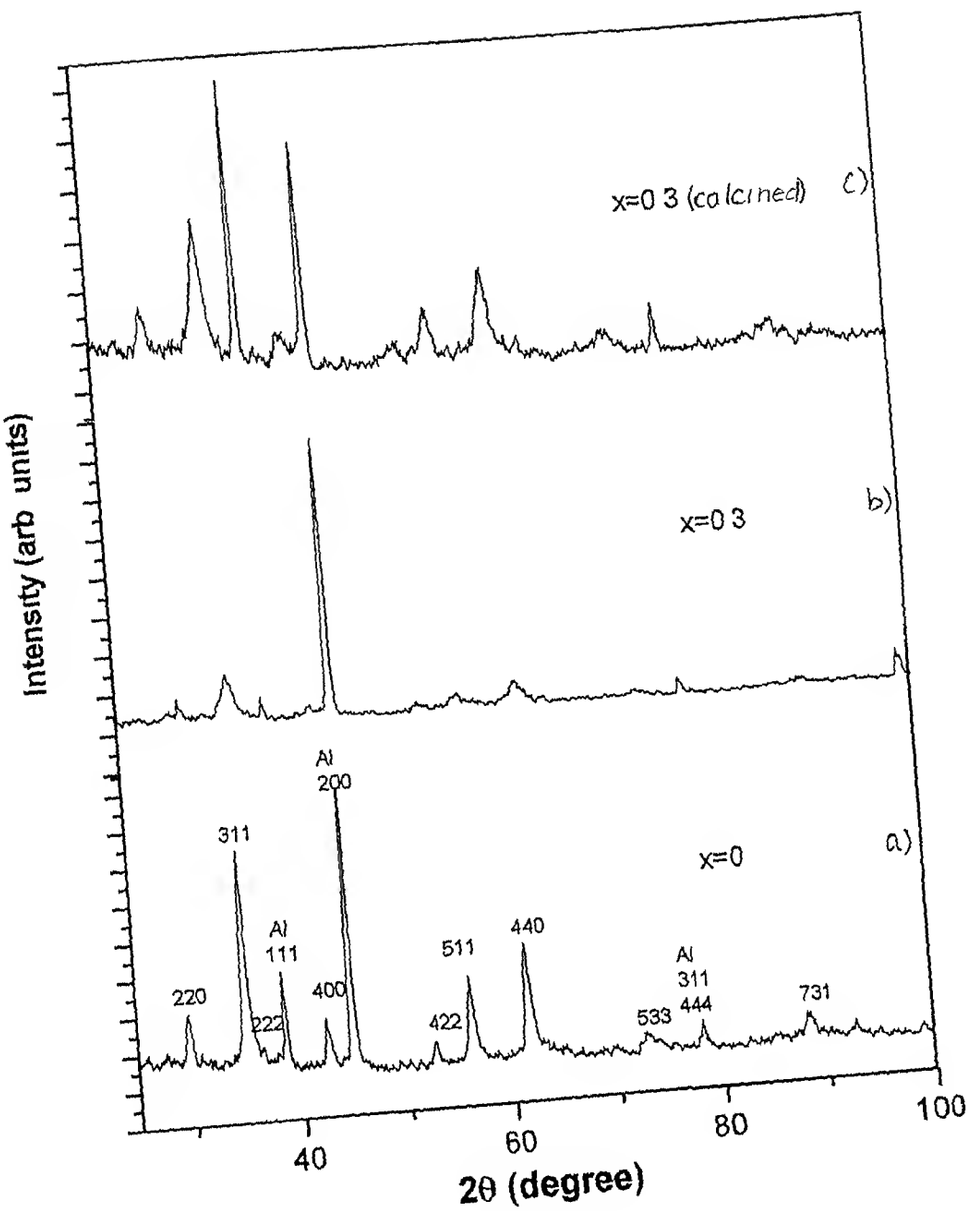

Fig 3 4 XRD pattern of a) pure $MnFe_2O_4$,b) $Mn_{1-x}Zn_xFe_2O_4$ x=0 3 after digestion at 90^{0}C for 90 mn, and c) $Mn_{1-x}Zn_xFe_2O_4$ x=0 3 after digestion at 90^{0}C for 90 mn and calcination at 200^{0}C for 2 h

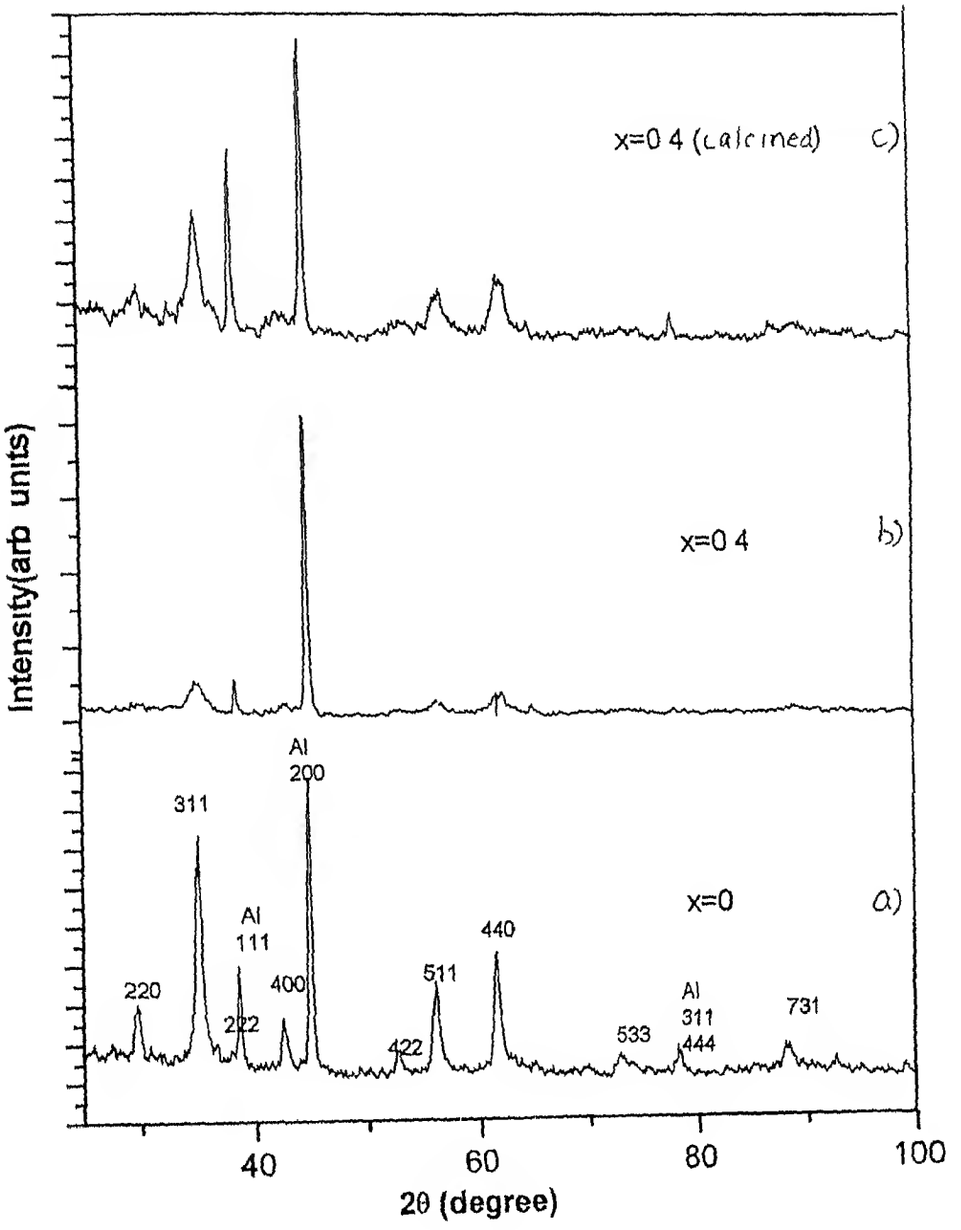

Fig 3 5 XRD pattern of a) pure $MnFe_2O_4$,b) $Mn_{1-x}Zn_xFe_2O_4$ x=0 4 after digestion at 90^0C for 90 mm and c) $Mn_{1-x}Zn_xFe_2O_4$,x=0 4 after digestion at 90^0C for 90 mm and calcination at 200^0C for 2 h

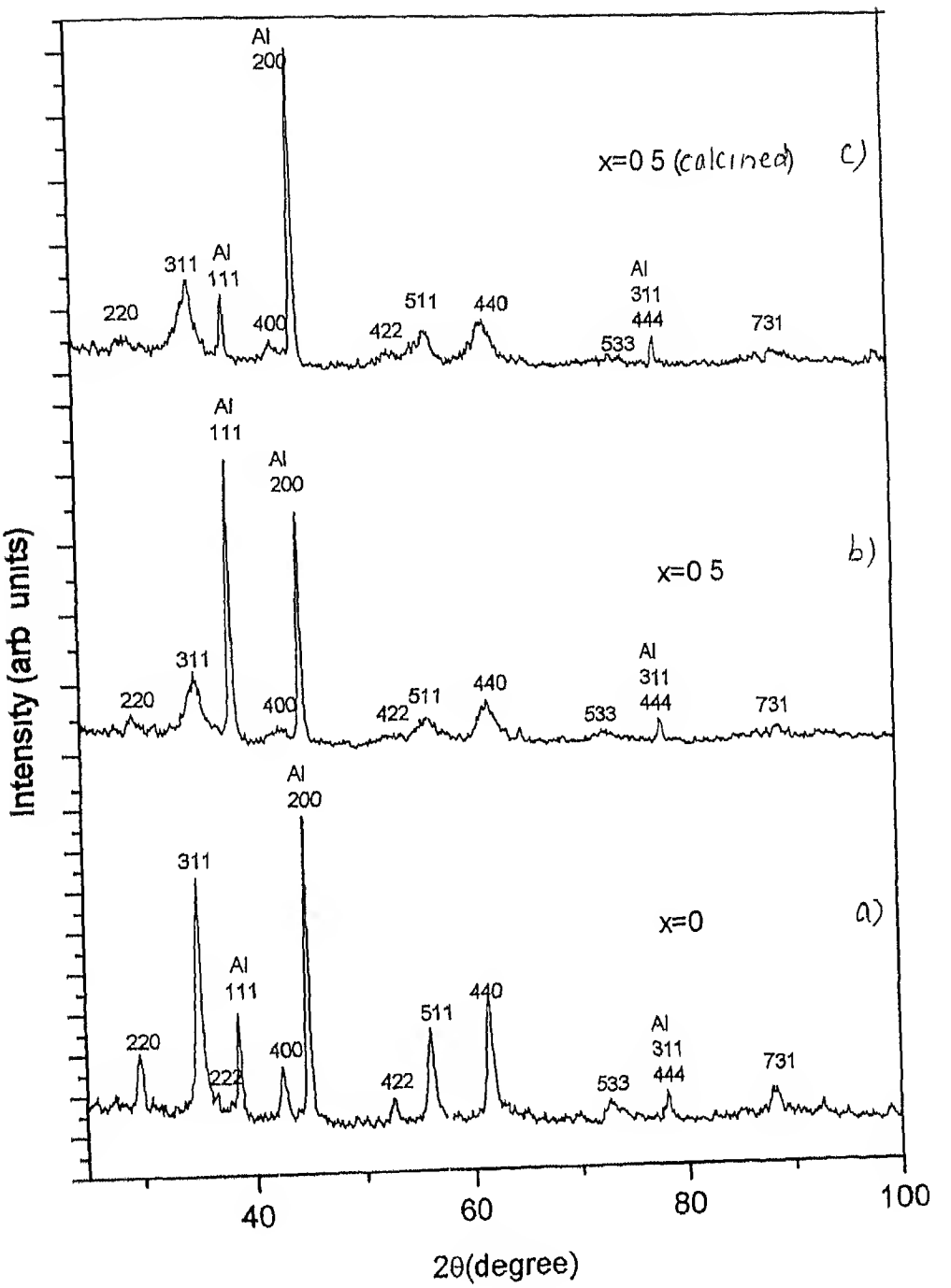

Fig 3 6 XRD pattern of a) pure $MnFe_2O_4$,b) $Mn_{1-x}Zn_xFe_2O_4$ x=0 5 after digestion at 90^{0}C for 90 min, and c) $Mn_{1-x}Zn_xFe_2O_4$,x=0 5 after digestion at 90^{0}C for 90 min and calcination at 200^{0}C for 2 h

3 2 TEM studies

Transmission electron micrograph and corresponding selected area diffraction (SAD) of $MnFe_2O_4$ are shown in Fig 3 7 A SAD pattern of a standard gold sample was also recorded under the same conditions for the calibration purpose (Fig 3 8) The radii relative intensities and indexing of diffraction rings of gold are given in Table 3 6 The value of camera constant was found as 6 77 mm (Å), taking the lattice parameter of gold as 4 0783 Å

Table 3 6 Electron diffraction data of standard gold sample

S No	Radius (mm)	Relative intensity	hkl
1	2 875	Very strong	111
2	3 335	Strong	200
3	4 700	Very strong	220
4	5 475	Strong	311
5	5 725	Weak	222
6	7 225	Weak	331
7	7 425	Weak	420
8	8 125	Strong	422
9	8 625	Weak	511, 333
10	9 400	Very weak	440
11	9 825	strong	531

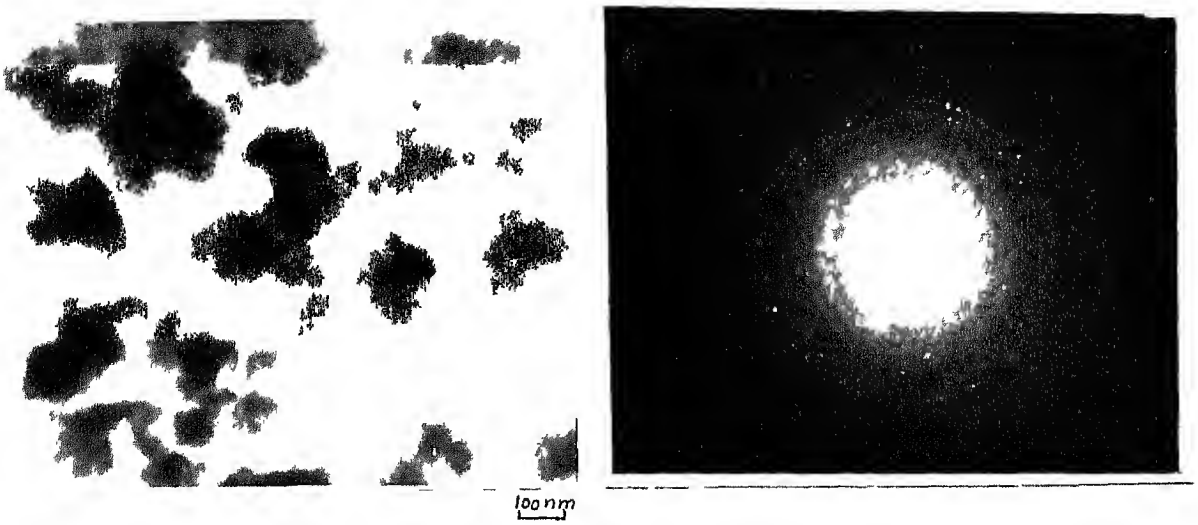

Fig 3 7 a) Transmission electron micrograph and b)corresponding diffraction pattern of $MnFe_2O_4$

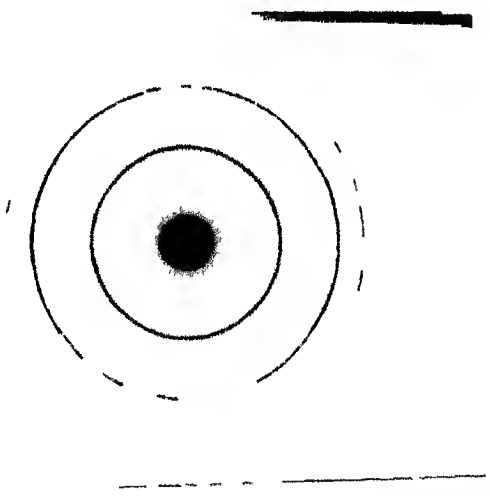

Fig 3 8 Diffraction pattern of gold sample

Fig 3 9 depicts some typical transmission electron micrograph of $Mn_{0.8}Zn_{0.2}Fe_2O_4$ The fine crystallites can be clearly seen disposed in the microstructure The SAD patterns are depicted in Fig 3 10 The data obtained from SAD patterns of manganese ferrite of compositions $Mn_{1-x}Zn_xFe_2O_4$ (x=0 0 2) are listed in Table 3 7 and 3 8 The indexing show that there is a single phase present in the system that corresponds to f c c structure with lattice parameter as 8 50 Å and 8 45 Å for composition of x=0 and 0 2 respectively

Table 3 7 Electron diffraction data of $Mn_{1-x}Zn_xFe_2O_4$ with x=0

S No	Radius (mm)	Interplanar spacing (Å)	Hkl
1	2 25	3 01	220
2	2 75	2 40	222
3	3 20	2 12	400
4	4 15	1 63	511
5	4 50	1 51	440
6	5 20	1 30	533
7	6 15	1 10	731

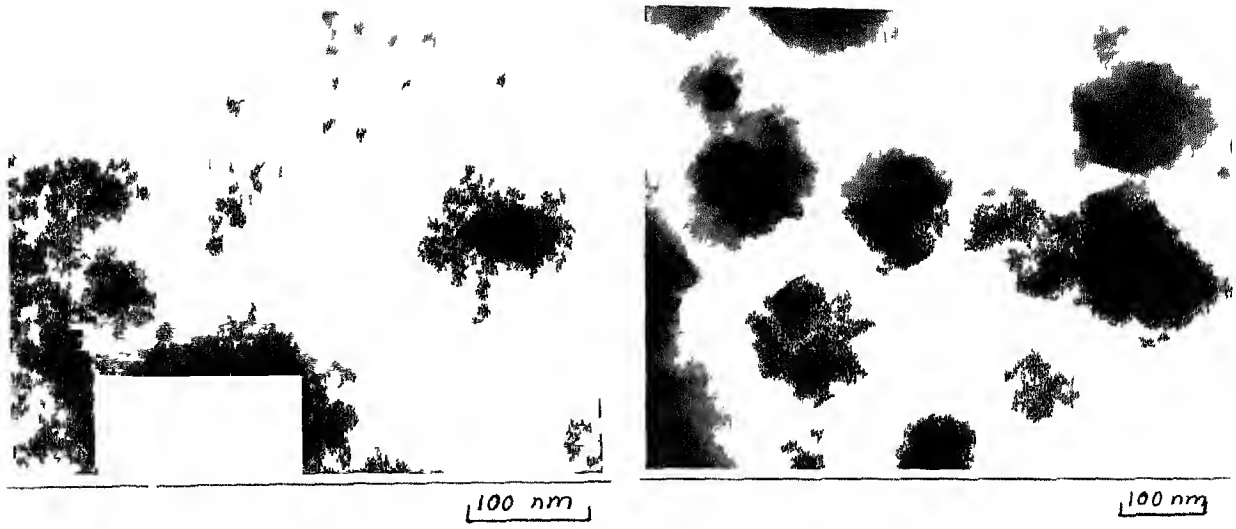

Fig 3 9 Transmission electron micrographs of $Mn_{0.8}Zn_{0.2}Fe_2O_4$ at a) 165 kX and b) 100 kX magnification

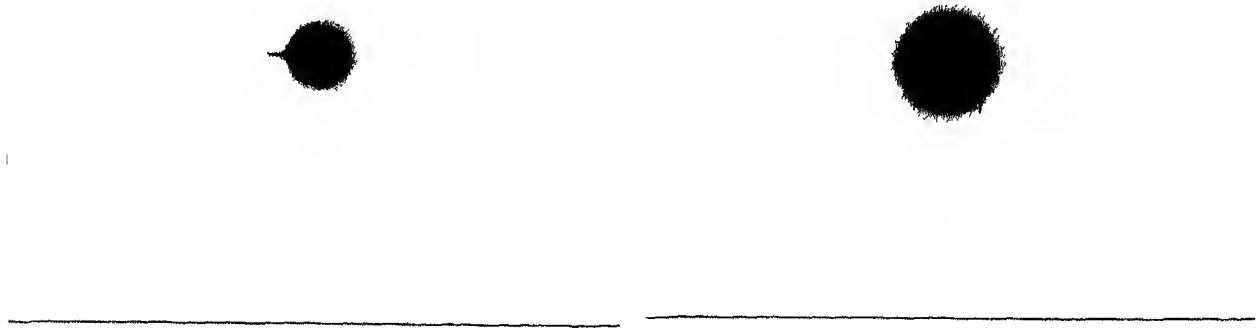

Fig 3 10 Diffraction patterns of $Mn_{0.8}Zn_{0.2}Fe_2O_4$

Table 3 8 Electron diffraction data for $Mn_{1-x}Zn_xFe_2O_4$ (x=0 2)

S No	Radius (mm)	Interplanar spacing (Å)	hkl
1	1 40	4 82	111
2	2 25	3 00	220
3	2 65	2 56	311
4	3 20	2 11	400
5	3 85	1 74	422
6	4 15	1 63	511
7	4 55	1 48	440
8	5 25	1 28	533
9	5 65	1 88	551
10	6 10	1 11	731

Some more electron micrographs showing tiny crystals of zinc substituted manganese ferrite with x=0 2 are presented in Fig 3 11

3 3 Surface area measurements

The BET specific surface area was measured as per description given in Section 2 2 3 The various parameters involved and the specific surface area values found are listed in Table3 9

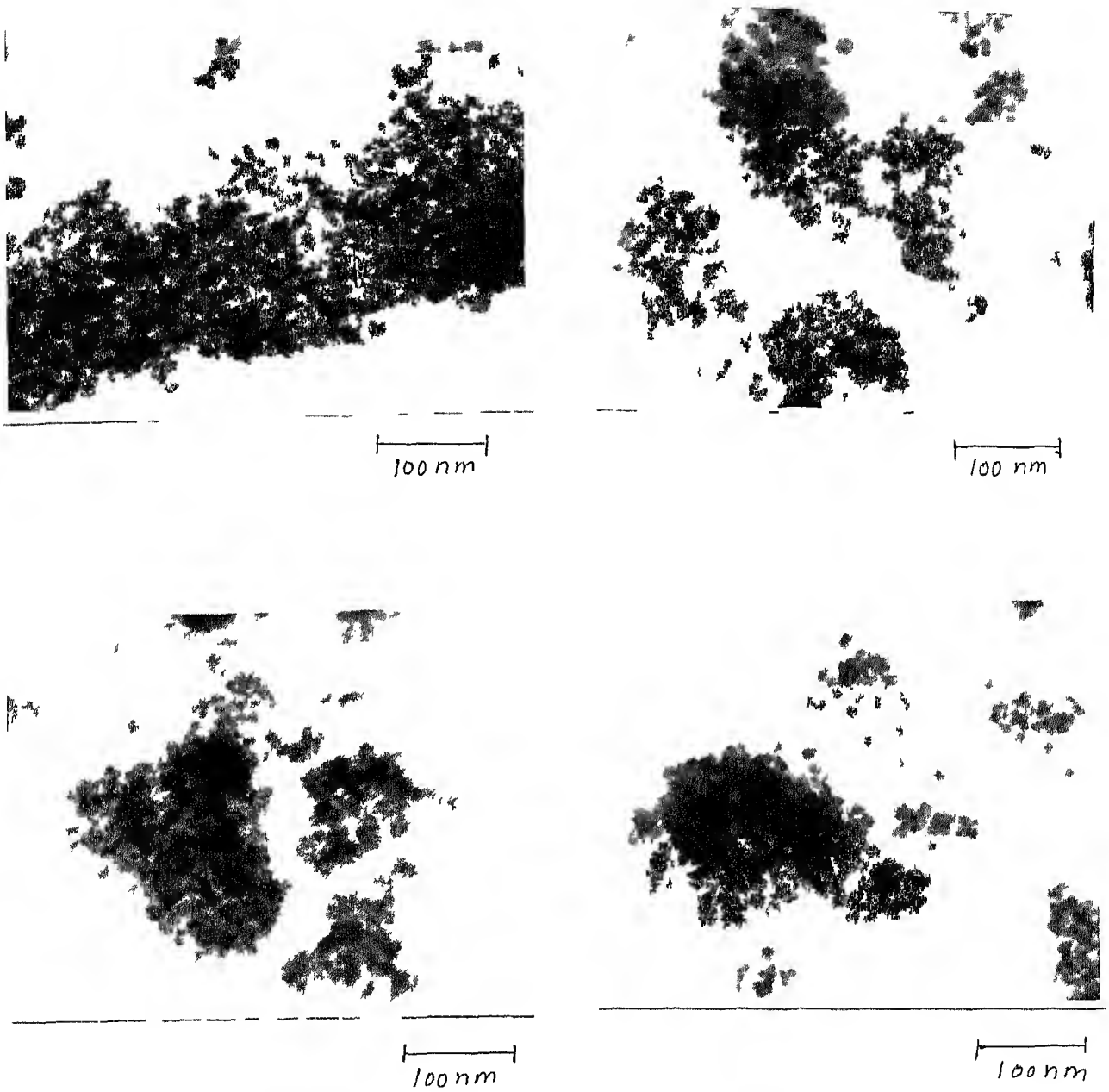

Fig 3 11 Transmission electron micrographs of $Mn_{0.8}Zn_{0.2}Fe_2O_4$ at 165Kx magnification

Table 3 9 Elapsed time used in the BET measurements, specific surface area and average particle size of $Mn_{1-x}Zn_xFe_2O_4$ samples

Zinc content (x)	Elapsed time (min)	Specific surface area (m^2/g)	Average particle diameter (nm)
0	65	118 2	10 2
0 1	59	141 2	8 4
0 2	80	148 7	7 8
0 3	37	190 0	6 2
0 4	65	194 2	6 0

Clearly surface area increases with increase of zinc concentration in $Mn_{1-x}Zn_xFe_2O_4$ system This implies that the average particle size is decreasing with zinc incorporation Considering the particles to be uniform and of spherical shape their average diameter (2r) can be estimated from the surface area data using the formula, diameter (2r) = 6 /(ρ × surface area) The values arrived at are listed in Table 3 9

3 4 Magnetic measurements

The magnetization vs magnetic field plots of pure manganese ferrite ($MnFe_2O_4$) and zinc substituted manganese ferrite of composition $Mn_{1-x}Zn_xFe_2O_4$ (x= 0 2 0 3 0 4 and 0 5) obtained at room temperature are shown in Fig3 12 Their saturation magnetization (M_s) values are listed in Table 3 10 The value ~ 43 emu/g of Ms for $MnFe_2O_4$ is much lower than that of the bulk (80 emu/g) It may be noted that the average particle diameter in the present case is ~ 10 2 nm The earlier reports indicate decrease of saturation magnetization with decrease in particle size For example values of Ms found are 24 4 emu/g and 54-79 emu/g for particle of average diameters 5 6 nm and 35 – 40 nm, respectively [24 26] This lowering of Ms has been attributed to (a) presence of a magnetic dead layer of a few Å (b) incomplete alignment of moments at the particle surface even at very high magnetic fields (c) Mn^{2+} to Mn^{3+} conversion, and (d) cation redistribution [21 23 26]

The M_s versus zinc content (x) data (Table 3 10) clearly reveal that the saturation magnetization is invariably lower than that of pure manganese ferrite But Ms initially increases with x atleast for x=0 3 and 0 4, but, decreases drastically for x=0 5from that of x=0 2 i e increase of zinc content

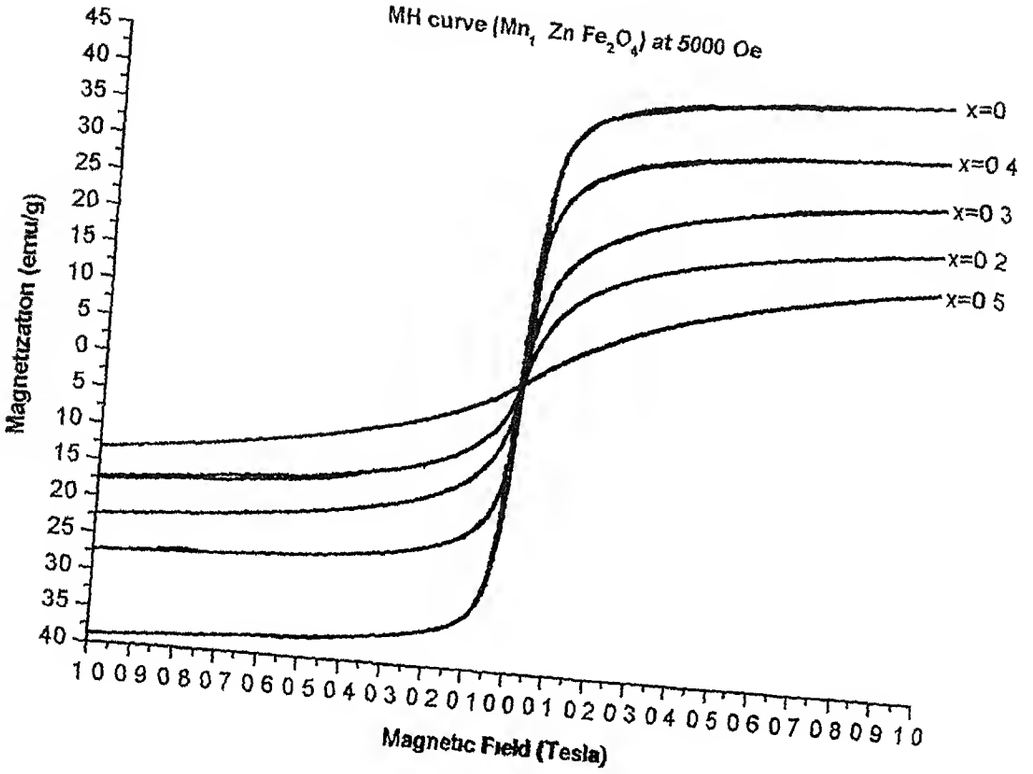

Fig 3 12 Magnetization versus applied field curve for zinc substituted manganese ferrite $Mn_{1-x}Zn_xFe_2O_4$ (x=0 0 2, 0 3 0 4, and 0 5)

Table 3 10 Saturation magnetization of $Mn_{1-x}Zn_xFe_2O_4$ for various zinc content (x)

Amount of zinc substitution (x)	Saturation magnetization Ms (emu/g)
0	42 98*
0 2	22 15
0 3	28 80
0 4	35 16
0 5	16 94

- The value cited in the literature for saturation magnetization (Ms) is 80 emu/g

Pure manganese ferrite is structurally described [31] as $(Mn_{0.8}Fe_{0.2})(Mn_{0.2}Fe_{1.8})O_4$ general formula being AB_2O_4 where A and B represent tetrahedral and octahedral sites in close packed layers of oxygen ions and meant for divalent and trivalent metal ions respectively for a normal spinel Alternatively the general formula can be written as $B(AB)O_4$ for the case of inverse spinel In this trivalent ions(B) occupy tetrahedral sites while divalent ions(A) and the remaining trivalent ions (B) assume octahedral positions In both normal and inverse spinel there are in all 8 tetrahedral and 4 octahedral positions per formula unit of AB_2O_4 Of them only one tetrahedral and two octahedral sites are filled Rest of the sites remain vacant The unit cell contains eight unit cells each of one AB_2O_4 formula unit with different disposition of filled sites (i e one tetrahedral and two octahedral) In case of $MnFe_2O_4$ manganese and iron ions assume positions in a mixed manner in tetrahedral and octahedral sites i e cations in first bracket $[Mn_{0.8}Fe_{0.2}]$ occupy tetrahedral void (or A site) while those in second bracket $[Mn_{0.2}Fe_{1.8}]$ fill octahedral void(or B site) Also disposition of A and B ions is such that their magnetic moments are directed antiparallel to each other [11] Thus, the net magnetic moment results due to difference in their respective contribution Zn^{2+} incorporation is intended to replace Mn^{2+} ion in $MnFe_2O_4$ Thus there are two possibilities with $[Mn_{0.8}Fe_{0.2}]$ $[Mn_{0.2}Fe_{1.8}]$

0_4 description First Zn^{2+} may go to B site upto x=0 2 and then to A site beyond x > 0 2 Second it may be replace Mn^{2+} from A site initially upto a certain x and start assuming B site there after The spin-only magnetic moments of Mn^{2+} Mn^{3+} Fe^{2+} Fe^{3+} and Zn^{2+} are 5 71 μ_B 4 98 μ_B 4 98 μ_B 5 91 μ_B and zero respectively, μ_B stands for the Bohr magneton Applying these considerationstogether with that the spin of A and B sites are antiparallel to each other their net contribution to saturation magnetization keeps on increasing with zinc content in the first case a result contrary to the present observation In second case the magnetic moment of A site decreases with zinc incorporation while that of B site remains constant upto a certain stage This means that the difference between the magnetic moments of two sites should increase When zinc begins to go to B site one expects decrease in the net magnetic moment as contribution of B site gets affected adversely This is what one observes in the present data The saturation magnetization initially increases with increase in zinc content (i e, for x=0 3 and 0 4), but,decreasesdrastically for x= 0 5 The above approach when used for $[Mn_{0\,8}Fe_{0\,2}][Mn_{0\,2}Fe_{1\,8}]\ 0_4$ the net spin magnetic moment contribution to saturation magnetization comes out to be ~ 121emu/g

The nature of hysteresis loop observed for pure $MnFe_2O_4$ samples suggest it to be a good soft magnetic material (Fig 3 13) But, with zinc incorporation no hysteresis loop could be observed (Fig 3 12) These findings indicate that the products assume increasing tendency of superparamagnetism with zinc incorporation Such a behaviour was also observed in $MnFe_2O_4$ particles of average size 5 nm[20] Therefore the superparamagnetism characteristics depicted in the preparations can be attributed to the decrease in particle diameter with increase in zinc content

The magnetization versus temperature (T) curves for the samples of $Mn_{1-x}Zn_xFe_2O_4$ (x=0, 0 2 0 3, 0 4 and 0 5) at a fixed magnetic field of 5000 Oe are shown in Fig 3 14 Similar curves at a fixed lower magnetic field of 500 Oe for compositions corresponding to x=0 0 2 and 0 4 are shown in Fig 3 15 Clearly the magnetization decreases continuously with increase of temperature upto a point beyond which the change is somewhat abrupt, indicative of ferromagnetic to paramagnetic transition Curie temperature (Tc) value determined by the intersection of tangent drawn at the point of highest slope in the magnetization versus temperature curve, with abscissa is 378°C as indicated in M_s versus T plot (Fig 3 15a) Thus, pure manganese ferrite samples show enhancement of Curie temperature by 78°C, known bulk value of Tc is 300°C [12] In

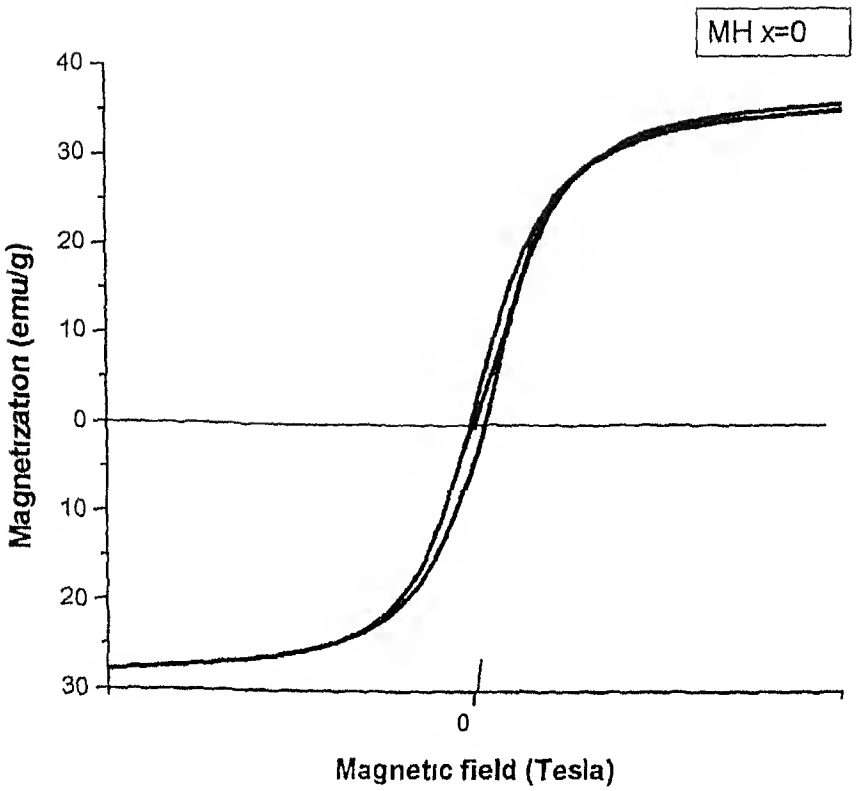

Fig 3 13 Magnetization versus applied field curve for manganese ferrite $MnFe_2O_4$

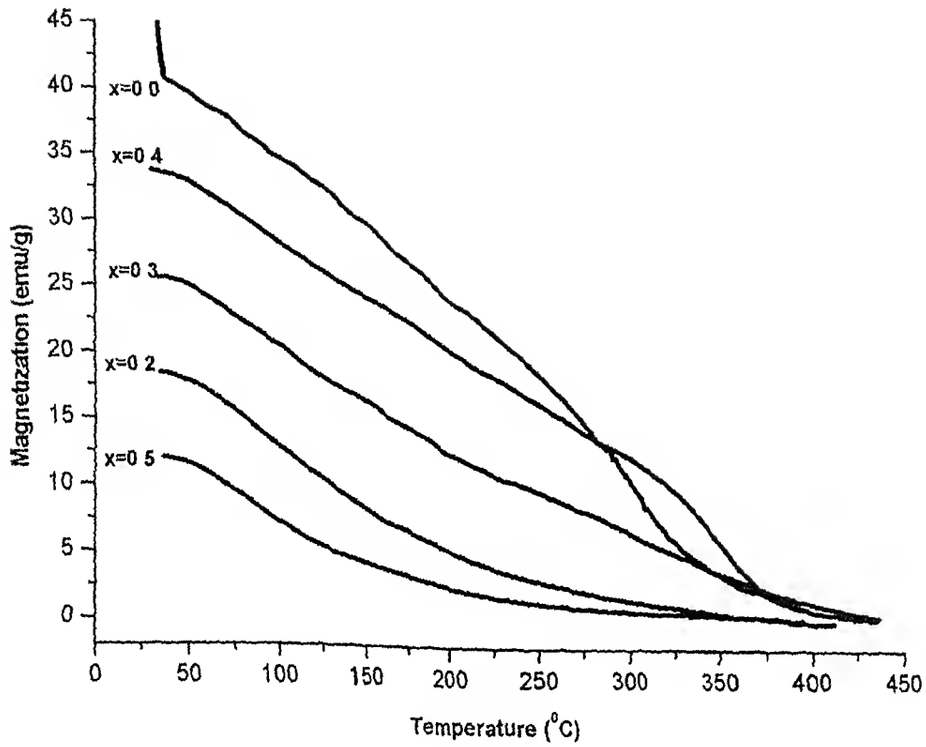

Fig 3 14 magnetization versus temperature curve at 5000Oe for $Mn_{1-x}Zn_xFe_2O_4$ (x=0, 0 2, 0 3, 0 4, and 0 5)

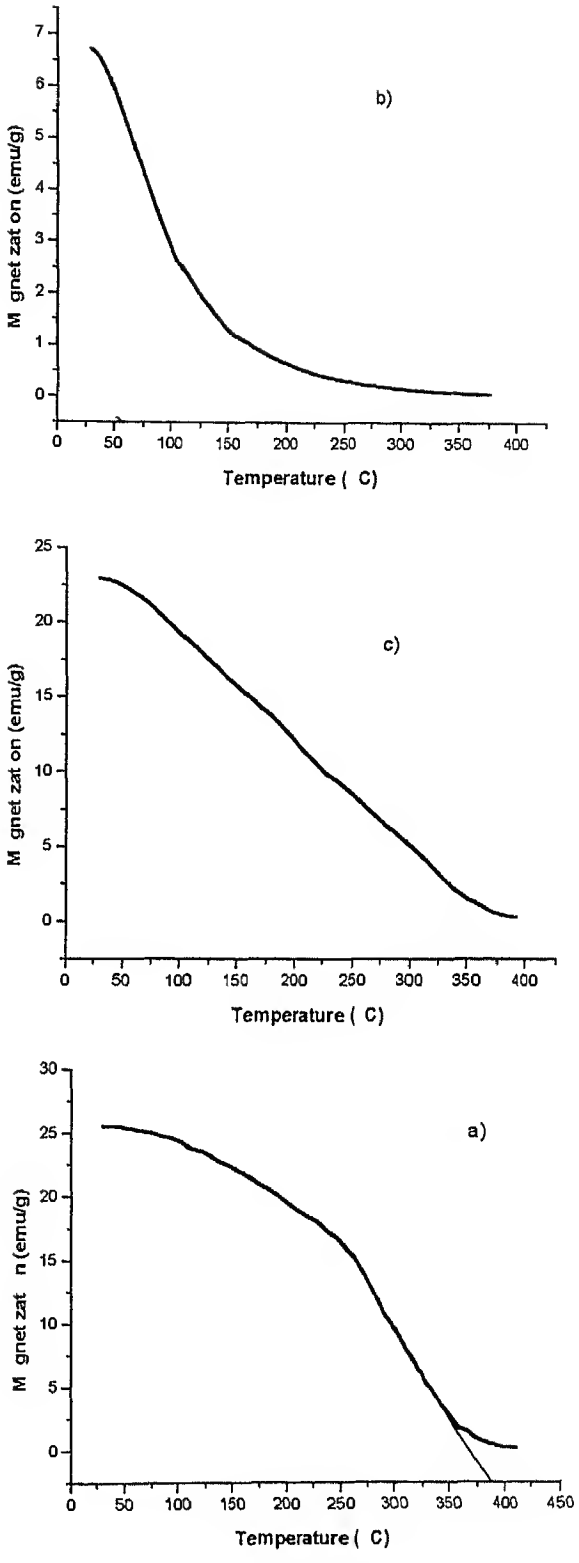

Fig 3 15 magnetization versus temperature curve at 500 Oe for $Mn_{1-x}Zn_xFe_2O_4$, a) x=0, b) x=0 2, c) x=0 4

case of zinc substituted manganese ferrite there is no clear transition Also Ms is continuously decreasing These features also support superparamagnetism tendency as found in fine particles earlier [20]

4 Conclusions

1 Nano crystalline particles (average diameter 6–10 2 nm) of pure and zinc substituted manganese ferrites of composition $Mn_{1-x}Zn_xFe_2O_4$ ($0 \leq x \leq 0\ 5$) can be prepared by coprecipitation of metal salts taking sodium hydroxide as a reaction agent followed by digestion at 90^0C for 90 minutes and calcination at 200^0C for 2 h

2 The products exhibit a single phase having an f c c structure with lattice parameter decreasing with increasing zinc content (the value being 8 503±0 001A^0 and 8 419±0 001A^0 for x = 0 and 0 5 respectively) possibly due to smaller size of Zn^{2+} in comparison to Mn^{2+} ion (radii being 0 83A^0 and 0 91A^0 respectively)

3 BET specific surface area of ferrite samples increases from 118 2 to 194 2 m^2/g for zinc content (x) increase from zero to 0 4 - indicative of emergence of crystallites of progressively smaller average size

4 $MnFe_2O_4$ particles exhibit a hysteresis loop of soft magnet They correspond to low saturation magnetization Ms (~ 42 98 emu/g) and high Curie temperature T_c (378^0C) in comparison to bulk values being Ms=80 emu/g and T_c =300^0C These characteristics can be attributed to small particle size cation redistribution besides presence of a magnetic dead layer on the surface

5 Zinc substitution leads to overall lowering of saturation magnetization for samples $Mn_{0\ 8}Zn_{0\ 2}Fe_2O_4$ depicting a value of 22 15 emu/g only With further increase of zinc content M_s value initially increases to 28 80 emu/g and 35 16 emu/g for x=0 3 and 0 4 respectively, but, decreases sharply later to 16 94 emu/g for x=0 5 Such a trend can be explained on the basis of gradual decrease in particle size and/or cation redistribution

References

01 A Morisako M Matsumoto and M Naoe *Sputtered hexagonal Ba ferrite films for high density magnetic recording media* J Appl Phys 79 4881 4883 (1996)

02 D E Speliotis *Performance of MP+ and BaFe+ tapes in high density recording applications* IEEE Trans on Magnetics 31 2877 2882 (1995)

03 T Fujiwara and T Corporation *Magnetic properties and recording characteristics of barium ferrite media (invited)* IEEE Trans on Magnetics 23 3125 3130 (1987)

04 D E Speliotis *Media for high density magnetic recording* IEEE Trans on Magnetics 20 669 674 (1984)

05 V Neilsen P Brauer F Primdahl T Risbo J L Jorgensen C Boe M Deyerler S Baueraisen *A high – precision triaxial fluxgate sensor for a space applications layout and choice of materials* Sensors and Actuators A 59 168 176 (1997)

06 Long Yi Li Chunhe Li Shimo Pan Huaining Lan Cuiling Zhang Liang *New application of the magnetic material in the cryogenic engineering Study of the magnetic compounds* $Er(NiCo)_2$ *for cryogenic regenerator* J of functional materials 26 341 343(1995)

07 J C H Spence *Surface imaging techniques and magnetic materials* Materials Science and Engineering B Solid State Materials for Advance Technology B3 421 425 (1989)

08 Z G M Lacava R B Azevedo E V Martins L M Lacava M L L Freitas V A P Garcia C A Rebula A P C Lemos M H Sousa F A Tourinho M F Da Silva P C Morais *Biological effects of magetic fluids toxicity studies* 201 431 434(1999)

09 J Ding T G McCormick R Street *Formation of Spinel Mn ferrite during mechanical alloying* J Magn Magn Mater 171 309 314 (1997)

10 A F Bakuzis, P C Morais *On the origin of the surface magnetic anisotropy in manganese ferrite nanoparticles* J Magn Magn Mater 226 1924-1926 (2001)

11 B D Cullity *"Introduction of magnetic materials* Addison Wesley London(1972) Ch 1 Ch 6

12 Francois Cardarelli *Materials Handbook* Springer Verleg London (2000) p 280 283 284 285 288

13 C N Chinnasamy A Narayanasamy N Ponpandian R Justin joseyphus B Jeyadevan K Tohji, K Chattopadhyay *Grain size effect on the Neel temperature and magnetic properties of nanocrystalline* $NiFe_2O_4$ *spinel* J Magn Magn Mater 238 281 287 (2002)

14 N M Borisova, Z V Golubenko, T G Kuzmicheva L P Olkhovik and V P Shabatin *Optimization principles for preparation methods and properties of fine ferrite materials* J Magn Magn Mater 114 317 328 (1992)

15 C Sudakar G N Subbanna and T R N Kutty *Nanoparticles of banum ferrite by gel to crystallite conversion and their magnetic properties* J of Electronics 6 2 123 134 (2001)

16 D Ramababu *An efficient process for synthesis of* $Yba_2Cu_3O_7$ Japanese Journal of Applied Physics 29 507 508 (1990)

17 Zheng Yang Hua Xian Zeng De Hua Han Jian Zhong Liu and Sheng Li Geng *Morphological structural and magnetic charatensation of Co Ti and Co Sn substituted Ba –ferrite particles for magnetic recording* J Magn Magn Mater 115 77 86 (1992)

18 L P Olkhovik N M Borisova A S Kamzin O G Fisenko *Radiothermal synthesis of fine banum ferrite powders and their properties* J Magn Magn Mater 154 365 368 (1996)

19 K haneda C Miyakawa and K Goto *Preparation of small particles of* $SrFe_{12}O_{19}$ *with high coercivity by hydrolysis of metal organic complexes* IEEE Trans on Magnetics 23 3134-3136 (1987)

20 Z X Tang C M Sorensen K J Klabunde G C Hadjipanayis *Preparation of manganese ferrite fine particles from aqueous solution* J of Colloidal and Interface Science 146 38 51 (1991)

21 Z X Tang C M Sorensen K J Klabunde G C Hadjipanayis *Size dependent curie temperature in nanoscale* $MnFe2O_4$ *particles* Phyical Review Letters 67 3602 3605 (1991)

22 M Zheng X C Wu B S Zou Y J Wang *Magnetic properties of nanosized* $MnFe_2O_4$ *particles* J Magn Magn Mater 183 152 156 (1998)

23 J P Chen C M Sorensen K J Klabunde G C Hadjipanayis E Devlin and A Kostikas *Size dependent magnetic properties of* $MnFe_2O_4$ *fine particles synthesized by co precipitation* Physical Review B 54 9288 9296 (1996)

24 J Ding P G Mccormick R Street *Formation of spinel Mn ferrite during mechanical alloying* J Magn Magn Mater 171 309 314 (1997)

25 M H Mahmoud C M Williams J Cai I Siu and J C Walker *Investigation of Mn ferrite films produced by pulsed laser deposition* J Magn Magn Mater (Article in press)

26 G Balaji N S Gajbhiye G wilde J Weissmuller *Magnetic properties of* $MnFe_2O_4$ *particles* J Magn Magn Mater (Article in Press)

27 G U Kulkarni K R Kannan T Arunarkavalli and C N R Rao *Particle size effects on the value of Tc of* $MnFe_2O_4$ *evidence for finite size scaling* 49 724 727 (1994)

28 R V Upadhyay, K J Davies S Wells S W Charles *Preparation nad charactenzation of ultra fine* $MnFe_2O_4$ *and* $Mn_xFe_{1-x}O_4$ *spinel systems II Magnetic fluids* J Magn Magn Mater 139 249 254 (1995)

29 C Rath K K Sahu S Anand S K Date N C Mishra R P Das *Preparation and charactenzation of nanosize Mn Zn ferrite* J Magn Magn Mater 202 77 84(1999)

30 J L Lopez H D Pfannes R Paniago F A Tourinho *Influence of particle size on supermagnetic relaxation of $MnFe_2O_4$ particles in ferrofluids* 226 1878 1880 (2001)

31 F S Galasso *Structure and properties of inorganic solids* Pergamon Press Oxford p 8 11 217 222 226

32 Rezlescu L Sachelarie P D Popa and N Rezlescu *Effect of substitution of divalent ions on the electrical and magnetic properties of Ni Zn Me ferrites* IEEE Transactions on Magnetics 30 3962 3967(2000)

33 *Powder Diffraction File Set 6 10 (Revised)* Inorganic Volume No PDIS 10IRB published by Joint Committee on Powder Difrraction Standards p 10 319